© 2021. Published by The Company of Biologists Ltd | Journal of Cell Science (2021) 134, jcs248732. doi:10.1242/jcs.248732

RESEARCH ARTICLE

Switching between blebbing and lamellipodia depends on the degree of non-muscle myosin II activity

Indranil Ghosh[1], Raman K. Singh[1,2], Manjari Mishra[3], Shobhna Kapoor[3] and Siddhartha S. Jana[1,*]

ABSTRACT

Cells can adopt both mesenchymal and amoeboid modes of migration through membrane protrusive activities, namely formation of lamellipodia and blebbing. How the molecular players control the transition between lamellipodia and blebs is yet to be explored. Here, we show that addition of the ROCK inhibitor Y27632 or low doses of blebbistatin, an inhibitor of non-muscle myosin II (NMII) ATPase activity and filament partitioning, induces blebbing to lamellipodia conversion (BLC), whereas addition of low doses of ML7, an inhibitor of myosin light chain kinase (MLCK), induces lamellipodia to blebbing conversion (LBC) in human MDA-MB-231 cells. Similarly, siRNA-mediated knockdown of ROCK and MLCK induces BLC and LBC, respectively. Interestingly, both blebs and lamellipodia membrane protrusions are able to maintain the ratio of phosphorylated to unphosphorylated regulatory light chain at cortices when MLCK and ROCK, respectively, are inhibited either pharmacologically or genetically, suggesting that MLCK and ROCK activities are interlinked in BLC and LBC. Such BLCs and LBCs are also inducible in other cell lines, including MCF7 and MCF10A. These studies reveal that the relative activity of ROCK and MLCK, which controls both the ATPase activity and filament-forming property of NMII, is a determining factor in whether a cell exhibits blebbing or lamellipodia.

KEY WORDS: Blebbing, Lamellipodia, Membrane protrusive activity, Non-muscle myosin II, Rho kinase, Myosin regulatory light chain kinase

INTRODUCTION

Blebs and lamellipodia both drive the efficient migration of cancer cells during metastasis (Paluch and Raz, 2013; Caswell and Zech, 2018), T cells during inflammation (Krummel et al., 2014; Dupré et al., 2015) and embryonic cells during development (Reig et al., 2014; Aman and Piotrowski, 2010). Bleb-based migration is a characteristic of amoeboid-like motility, whereas lamellipodia-mediated migration is a characteristic of mesenchymal-type motility. Blebs are spherical membrane protrusions that often undergo fast expansion–retraction cycles within a period of ∼120 s (Barry et al., 2015). Blebs are thought to be formed at regions of the cell surface where the plasma membrane detaches from the underlying cytoskeleton, either due to increased cortical actomyosin contractility at the point of detachment (Charras et al., 2006) or due to the weak and sparser cytoskeleton providing vulnerable sites to release intracellular pressure (Chikina et al., 2019b). In all cases, non-muscle myosin II (NMII) is found to be associated with actin filaments, not only with the cortical but also with the interior 'actin filaments' of the blebs, suggesting the importance of NMII in the bleb life cycle. NMIIs consist of one pair each of heavy chain (HC), regulatory light chain (RLC) and essential light chain (ELC) subunits (Coluccio, 2007; Berg et al., 2001; Golomb et al., 2004). RLC kinases and HC kinases regulate the ATPase activity and filament-forming properties of NMII for the execution of various cellular functions, such as migration, cytokinesis and adhesion (Vicente-Manzanares et al., 2009b).

In contrast, lamellipodia are the extension of the actin cytoskeleton at the leading edge of cells. During lamellipodia-mediated migration, cells generate two distinct actin networks at the lamellipodium and lamella. One assembles at the leading edge and disassembles within 1–3 µm, which promotes protrusion and retraction, respectively, of the leading edge at lamellipodia (Ponti et al., 2004; Giannone et al., 2004). The other network is involved in substrate adhesion and provides actomyosin contractility due to the presence of NMII at the lamella. Lamellipodia are enriched with Arp2/3 complex and ADF/cofilin, whereas lamellae are enriched with NMII and tropomyosin (Ponti et al., 2004). The migration of cells using lamellipodia proceeds by cycles of edge protrusion, adhesion and retraction within a period of ∼24 s (Giannone et al., 2007). NMII pulls the rear of the lamellipodial actin network, which causes upward bending, edge retraction and initiation of new adhesion sites. Hence, actin polymerization periodically builds a mechanical connection with NMII motors in the lamellipodium. However, the molecular mechanism behind the switching between blebbing and lamellipodia has not been fully explored.

Blebs and lamellipodia both recruit molecules required for their functions. Ankyrin B (also known as ANK2), protein 4.1 and myr3 (also known as MYO1E) are consistently present at the bleb membrane during expansion, whereas ezrin, α-actinin, coronin, and tropomyosin-4 (TPM4) are recruited at the retracting bleb membrane (Charras et al., 2006). Likewise, Arp2/3 complex, N-WASP (also known as WASL), VASP, Abi and many other molecules are localized at the lamellipodia. Lamellipodia membrane protrusive activity is regulated by the small GTPases Rac1 and Cdc42, which are activated by growth factor and integrin receptors (Small et al., 2002). These small GTPases activate the Arp2/3 complex through WASP (Wiskott-Aldrich syndrome protein) and WAVE (WASP-family verprolin-homologous protein) proteins to form a dense actin network at lamellipodia (Vicente-Manzanares et al., 2009a). Although the molecules involved in blebbing and the formation of lamellipodia are well studied, the molecular players that control the transition between the two membrane protrusions are poorly understood.

In this study, we decipher the key molecular players involved in the transition between blebbing and lamellipodia at the single-cell

[1]School of Biological Sciences, Indian Association for the Cultivation of Science, Kolkata 700032, India. [2]Weizmann Institute of Science, Rehovot 7610001, Israel. [3]Department of Chemistry, Indian Institute of Technology – Bombay, Mumbai 400076, India.

*Author for correspondence (bcssj@iacs.res.in)

S.S.J., 0000-0003-0897-7978

Handling Editor: Andrew Ewald
Received 12 May 2020; Accepted 19 November 2020

Journal of Cell Science (2021) 134, jcs248732. doi:10.1242/jcs.248732

level in normal human breast cells and in breast cancer cell lines of different metastatic potential. We observe that pharmacological or genetic inhibition of ROCK induces the transition from blebbing to lamellipodia, whereas inhibition of myosin light chain kinase (MLCK) induces the transition from lamellipodia to blebbing, suggesting that different signalling inputs converge in maintaining the NMII activity, which governs the membrane protrusive activity of the cell.

RESULTS

Blebbing and lamellipodia formation depend on NMII activity

Previous studies have established that actomyosin contractility and actin protrusivity at the edge of cells drive blebbing and lamellipodial activities of the plasma membrane, respectively (Bergert et al., 2012). The presence of folded NMII monomers and their mini filaments at the lamellipodium and lamella (Shutova et al., 2014), and the debate over whether NMII activity is needed for blebbing and formation of lamellipodia (Chikina et al., 2019b; Oakes et al., 2018), prompted us to re-assess the importance of NMII in such essential membrane protrusive activities. We treated human breast metastatic tumour MDA-MB-231 cells, which show both blebbing and lamellipodial membrane protrusive activities on glass surfaces, with the NMII inhibitor (−) blebbistatin (the active enantiomer of blebbistatin) at 0–30 µM, and captured time-lapse images at 20 s intervals for 15–25 min. Fig. S1A,B show time-lapse images of blebbing and lamellipodial cells in the presence of 20 and 30 µM (−) blebbistatin. Membrane protrusions in both blebbing and lamellipodial MDA-MB-231 cells were almost stopped within ∼5–10 min of 20 or 30 µM (−) blebbistatin addition (Movies 1,2). Lamellipodial structures (sheet-like) were lost and finger-like structures appeared within 5–10 min (Fig. S1B, Movie 2). The majority of the blebbing or lamellipodial cells were unable to return to their original states after 20 and 30 µM (−) blebbistatin treatments were washed out (Movies 3,4). In contrast, blebbing and lamellipodial cells showed different responses at lower doses of (−) blebbistatin. We selected 1, 2.5, and 10 µM (−) blebbistatin, because at these concentrations NMII activity has been shown to be inhibited by 20%, 50% and 80%, respectively, in a cell-free system (Straight et al., 2003). Fig. 1A shows that blebbing was converted to lamellipodia in the presence of 2.5 µM (−) blebbistatin within ∼10 min, whereas blebbing activity remained unchanged in the presence of 1 µM (−) blebbistatin (also see Movies 5,6). This blebbing to lamellipodia conversion (BLC) was reversed (i.e. lamellipodia to blebbing conversion; LBC), when 2.5 µM (−) blebbistatin was washed out from the medium (Movie 7). On the other hand, addition of 2.5 µM (−) blebbistatin could not stop lamellipodial membrane protrusive activity (Movie 8). However, both blebbing and lamellipodial membrane activities were completely stopped and the cells became rounded in ∼10 min (Fig. 1B; Movies 9,10) in the presence of 10 µM (−) blebbistatin, a response similar to that observed with 20 or 30 µM (−) blebbistatin treatment. Lamellipodial cells showed finger-like structures, which seemed to be actin filaments wrapped with plasma membrane (Fig. S1C). Unlike the response following 20 and 30 µM (−)

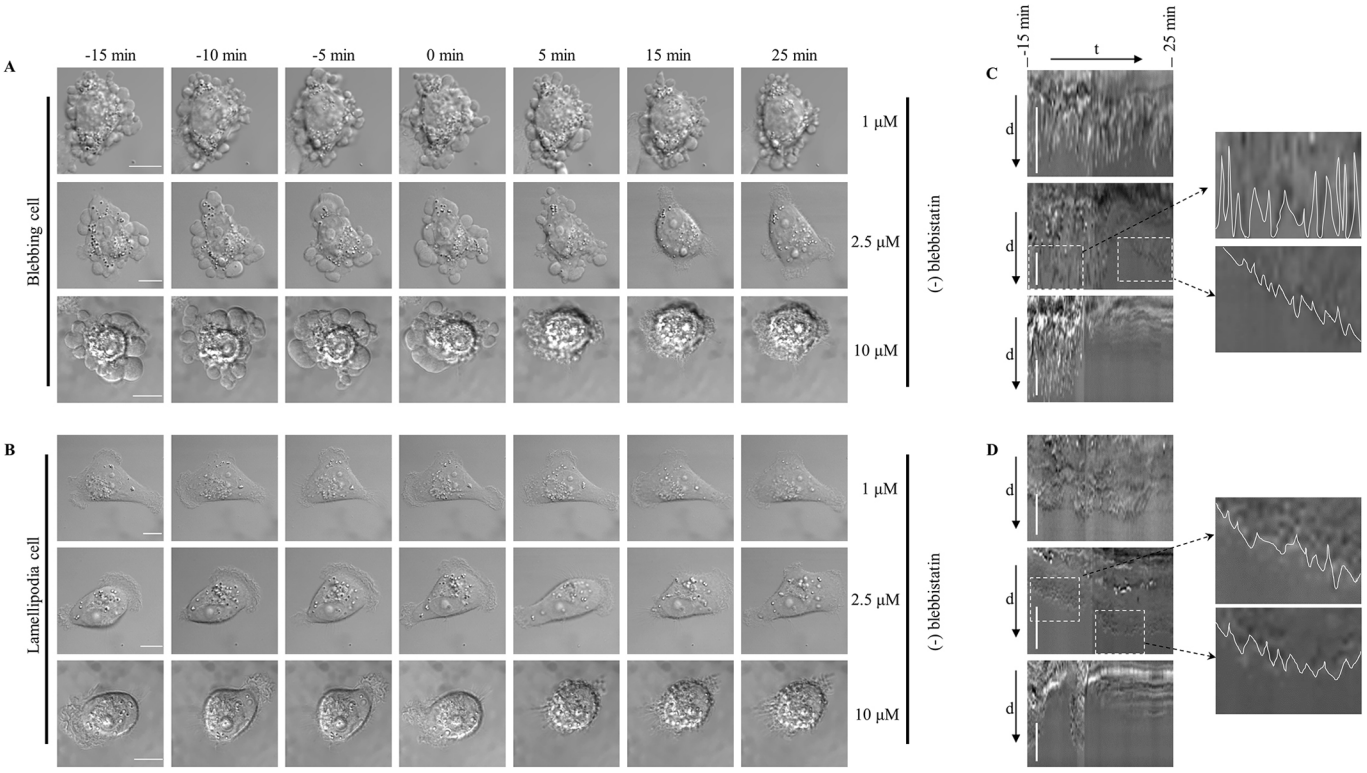

Fig. 1. NMII activity is required for blebbing and lamellipodia membrane protrusive activities. (A,B) Time-lapse images of blebbing (A) and lamellipodial (B) MDA-MB-231 cells treated with 1–10 µM (−) blebbistatin, as indicated. Images were captured for 15 min before and for 25 min after the addition of (−) blebbistatin. Note that blebs are converted to lamellipodia, whereas lamellipodia remain unchanged in the presence of 2.5 µM (−) blebbistatin. (C,D) Representative DIC kymographs of corresponding (−) blebbistatin-treated blebbing (C) and lamellipodial (D) cell edges. Regions of interest shown in the kymograph of 2.5 µM (−) blebbistatin-treated cells (dashed boxes) have been magnified to demonstrate the differences between bleb and lamellipodia edges. White lines indicate the rapid fluctuation of the cell edge in the blebbing membrane with almost no net distance movement, compared with slow but steady advancement of the lamellipodium membrane. $n \geq 20$ cells for each dose from three independent experiments. Scale bars: 10 µm (A,B), 5 µm (C,D).

Journal of Cell Science (2021) 134, jcs248732. doi:10.1242/jcs.248732

blebbistatin treatments, 40% of blebbing cells were able to return to the original blebbing phenotype, and all the lamellipodial cells were able to return to the lamellipodial phenotype, when 10 µM (−) blebbistatin was washed out (Movies 11,12). Interestingly, both blebbing and lamellipodial protrusions remained unaffected in the presence of either 2.5 µM (+) blebbistatin (the inactive enantiomer of blebbistatin) or vehicle control (0.2% DMSO; Fig. S1D–G, Movies 13,14).

We carried out kymograph analysis to examine the kinetics of conversion of membrane protrusive activities in (−) blebbistatin-treated MDA-MB-231 cells (Fig. 1C,D, Table 1). A representative differential interference contrast (DIC) kymograph shows that the edge of a blebbing membrane fluctuated with almost equal amplitude of protrusion and retraction, whereas both amplitudes were drastically reduced in the presence of 2.5 µM (−) blebbistatin (shown in magnified images) and there was progressive movement of the edge, which is a characteristic of lamellipodial membrane (Giannone et al., 2007, 2004). This BLC occurred in 13.44±0.95 min (mean±s.e.m.). In contrast, blebbing stopped within 9.52±0.69 min, and lamellipodial protrusion stopped within 7.09±0.2 min, in the presence of 10 µM (−) blebbistatin, suggesting that blebbing requires more NMII activity than lamellipodia.

BLC was also observed in MCF7 (Fig. S2) and MCF10A (Fig. S3) cells in the presence of 5 µM (−) blebbistatin, and both cells needed ≥20 µM (−) blebbistatin to stop blebbing or lamellipodial protrusions. These data suggest that both blebbing and lamellipodial membrane protrusive activities of a cell type are dependent on the degree of available NMII ATPase activity and filament-forming property.

ROCK inhibitor induces BLC

Membrane protrusive activity has been shown to be dependent on the activity of small GTPases Rac and Rho, which control actin polymerization, actomyosin contractility and cell–matrix adhesion by modulating the activity of ROCK and MLCK (Palamidessi et al., 2008; Sanz-Moreno et al., 2008; Sahai and Marshall, 2003; Totsukawa et al., 2000; Kassianidou et al., 2017; Kazakova et al., 2020). Both these enzymes can phosphorylate RLC resulting in the formation of active, unfolded and filament-competent forms of NMIIs. In addition, association and dissociation of the active NMII with the actin filament are also regulated by HC phosphorylation, which is mainly caused by casein kinase II (CKII), protein kinase C (PKC) and TRPM7 (Vicente-Manzanares et al., 2009b). We asked which kinase activity could be involved in regulating NMII dynamics during blebbing and lamellipodia conversion. Fig. 2A,B show frames from time-lapse movies of blebbing MDA-MB-231 cells treated with Y27632 (a known ROCK inhibitor) or ML7 (a known MLCK inhibitor) at different concentrations. We observed BLC when the blebbing cells were treated with Y27632 (even at low dose, 5 µM; Fig. 2A; Movies 15,16 with 5 and 20 µM Y27632, respectively), whereas blebbing remained almost unchanged in the presence of 5 µM ML7 (Movie 17) but stopped at higher doses (20–30 µM) within 5 min of its addition to the cells (Fig. 2B; Movie 18 with 20 µM ML7). Interestingly, BLC was not reversible whenY27632 was washed out from the medium (Movies 19,20 with 5 and 20 µM Y27632, respectively), whereas 20 µM ML7 washout from the medium resulted in a return to blebbing within 20 min (Movie 21). Because the BLC was not reversible in 5 µM Y27632 washout experiments, we further reduced the concentration to 0.1, 1 or 2 µM. At 0.1 µM Y27632, blebbing cells remained unchanged (Movie 22). At 1 µM Y27632, BLC was visible and was partially reversed 30 min after the drug was washed out, whereas BLC was not reversible in the same time period following treatment with 2 µM Y27632 (Movie 23), suggesting that ROCK may modulate NMII activity through other effectors during the conversion. Kymograph analysis (Fig. 2C,D) revealed that MDA-MB-231 cells underwent BLC within 2.8±0.15 min (mean±s.e.m.) in the presence of 5 µM Y27632. Blebbing cells became rounded within 6.13±0.37 and 5.8±0.28 min in the presence of 20 and 30 µM ML7 (Table 1), respectively.

Similarly, addition of Y27632 and ML7 resulted in BLC and inhibition of blebbing, respectively, in blebbing MCF7 and MCF10A cells (Fig. S4). Interestingly, when the cells were treated with HC kinase inhibitors, including 20 µM TG100-115, 20 µM Go 6976 and 20 µM TBBt (Movie 24), membrane protrusive activity in blebbing cells remained unchanged, suggesting that heavy chain phosphorylation by individual kinases is less likely to be involved in altering the disassembly and remodelling of NMII during BLC of blebbing cells. Taken together, these results suggest that BLC is dependent on the activity of NMII and ROCK, but not MLCK.

MLCK inhibitor induces LBC

In a similar way, lamellipodial cells were treated with the kinase inhibitors. Unlike the effects on membrane protrusive activity in blebbing cells, treatment of Y27632 and ML7 led to a differential response in lamellipodial cells. Addition of 5–30 µM Y27632 did not affect lamellipodia (Fig. 3A; Movie 25), whereas treatment with ML7 resulted in a dose-dependent response in lamellipodial cells. Fig. 3B shows a representative lamellipodial cell that was transiently converted to blebbing and returned back to lamellipodial

Table 1. Dose-dependent effect of inhibitors on blebbing and lamellipodial MDA-MB-231 cells

Inhibitor treatment	Blebbing cell response	Lamellipodial cell reponse
DMSO (vehicle)	NC (*n*=21)	NC (*n*=92)
1 µM (–) blebbistatin	NC (*n*=20)	NC (*n*=57)
2.5 µM (–) blebbistatin	BLC (13.44±0.96 min, *n*=27)	NC (*n*=70)
10–30 µM (–) blebbistatin	Stop (9.52±0.69 min for 10 µM, *n*=23) (T_n=41)	Stop(7.09±0.2 min for 10 µM, *n*=30) (T_n=106)
5–10 µM ML7	NC (T_n=58)	LBC(2.82±0.13 min for 10 µM, *n*=32) (T_n=121)
20–30 µM ML7	Stop (6.13±0.37 min for 20 µM, *n*=20) (T_n=61)	Stop (3.09±0.09 min for 20 µM, *n*=76) (T_n=262)
0.1 µM Y27632	NC (*n*=15)	NC (*n*=17)
1 µM Y27632	BLC (7.1±0.53 min, *n*=25)	NC (*n*=41)
2 µM Y27632	BLC (3.54±0.43 min, *n*=16)	NC (*n*=34)
5–30 µM Y27632	BLC (2.85±0.15 min for 5 µM, *n*=52) (T_n=138)	NC (T_n=231)
20 µM TG100-15	NC (*n*=29)	NC (*n*=60)
20 µM Go 6976	NC (*n*=42)	NC (*n*=66)
20 µM TBBt	NC (*n*=24)	NC (*n*=77)

Data for each treatment were collected from more than three experiments. BLC, blebbing to lamellipodia conversion; LBC, lamellipodia to blebbing conversion; NC, no conversion. T_n, total number of cells for a range of doses, as indicated; *n*, number of cells for a particular dose. Response times are shown as mean±s.e.m.

Journal of Cell Science (2021) 134, jcs248732. doi:10.1242/jcs.248732

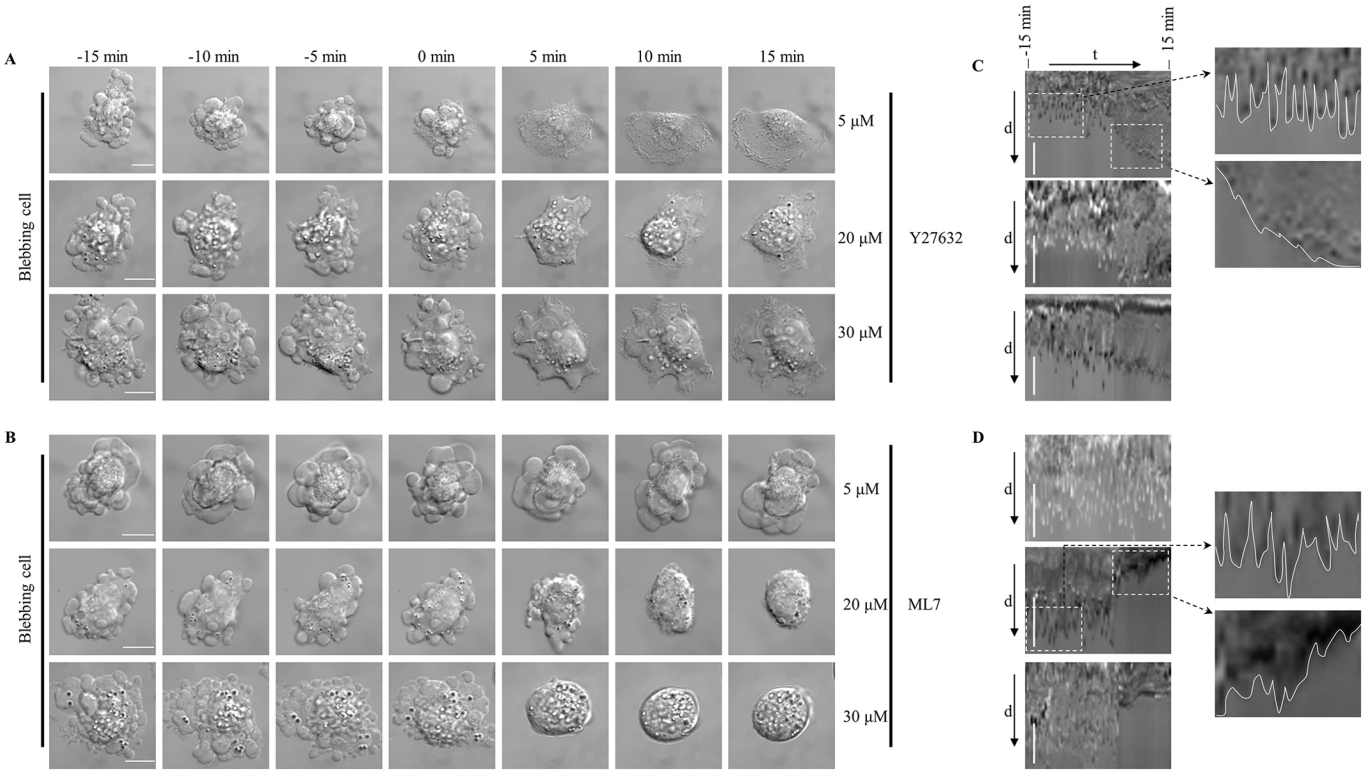

Fig. 2. Blebbing to lamellipodia conversion depends on ROCK activity. (A,B) Time-lapse images of blebbing cells in the presence of Y27632 (A) or ML7 (B) at the indicated concentrations. Images were captured for 15 min before and after the addition of inhibitors. Note that BLC was visible within 5 min after Y27632 treatment but not with ML7 treatment. Addition of ML7 stops blebbing, but no BLC was visible. (C,D) Representative DIC kymographs of corresponding blebbing cells treated with Y27632 (C) or ML7 (D). Regions of interest shown in the kymographs (dashed boxes) have been magnified to see the differences in blebbing edges between 5 µM Y27632- and 20 µM ML7-treated cells. White lines indicate the edges of blebbing membranes. $n \geq 20$ cells for each dose from three independent experiments. Scale bars: 10 µm (A,B), 5 µm (C,D).

protrusions within 10 min in the presence of 5 µM ML7 (Movie 26), and sustainable LBC was noticeable in the presence of 10 µM ML7 (Fig. 3B; Movie 27), which was followed by BLC when ML7 was removed (Movie 28). At higher doses (≥20 µM), lamellipodial membrane protrusive activity was completely abolished within 5 min (Fig. 3B; Movie 29). Interestingly, lamellipodia were again formed when 20 µM ML7 was washed out from the medium (Movie 30). From the kymograph analysis (Fig. 3C,D), we observed that treatment with 5 µM Y27632 did not affect lamellipodia, but 10 µM ML7 induced LBC within 2.8±0.13 min (mean±s.e.m.). Lamellipodial cells were rounded with no protrusions within 3.09 ±0.09 min and 2.7±0.08 min in the presence of 20 and 30 µM ML7, respectively (Table 1).

Similarly, treatment with ML7 generated LBC and no protrusions in lamellipodial MCF7 and MCF10A cells (Fig. S5). However, lamellipodia were unaffected by the presence of HC kinase inhibitors (20 µM TG100-15, 20 µM Go 6976 or 20 µM TBBt; Movie 31). Taken together, these data suggest that NMII dynamics in lamellipodia are regulated mainly by MLCK.

MLCK and ROCK are interlinked in BLC and LBC

Treatment with Y27632 caused BLC in blebbing cells but had no effect in lamellipodial cells, whereas treatment with low concentrations (10 µM) of ML7 caused LBC in lamellipodial cells but had no effect in blebbing cells. These findings prompted us to investigate the role of MLCK under ROCK-inhibited conditions and vice versa. First, we inhibited ROCK for 15 min followed by inhibition of MLCK for another 15 min and captured time-lapse images of blebbing and lamellipodial cells. Fig. 4A shows a representative blebbing cell that was converted to lamellipodial within 5 min of addition of Y27632, then subsequently converted to blebbing when ML7 was added (Movie 32). In contrast, lamellipodial protrusions were unchanged in the presence of Y27632, as seen in our earlier experiment (Fig. 3A), but stopped after the addition of ML7 (Fig. 4B; Movie 33), suggesting that lamellipodia may be maintained by MLCK activity under ROCK-inhibited conditions. Next, we reversed the conditions by inhibiting MLCK for 15 min followed by inhibition of ROCK for another 15–30 min. We observed that blebbing cells remained unchanged in the presence of ML7, but converted to lamellipodial cells when Y27632 was added. In contrast, lamellipodial cells showed blebbing in the presence of ML7, but returned to lamellipodia when Y27632 was subsequently added (Fig. 4C,D; Movies 34,35), suggesting that MLCK is activated in ROCK-inhibited conditions and vice versa. This activation of MLCK or ROCK meant that these kinases were less likely to be inhibited by the existing ML7 or Y27632, respectively. Taken together these data suggest that inhibition of ROCK induces activity of MLCK (a downstream effector of RacGTP), which maintains lamellipodia, whereas inhibition of MLCK induces activity of ROCK (a downstream effector of RhoGTP), which maintains blebbing.

NMII activity in blebbing and lamellipodial cells

We assessed myosin II activity in blebbing and lamellipodial cells by measuring the ratio of phosphorylated RLC (pRLC) to RLC in the presence or absence of kinase inhibitors and following genetic loss of these kinases. Genetic loss of ROCK and MLCK was carried out using an RNA interference (RNAi) approach (Keller et al., 2012; Chikina et al., 2019a) with endoribonuclease-prepared

Journal of Cell Science (2021) 134, jcs248732. doi:10.1242/jcs.248732

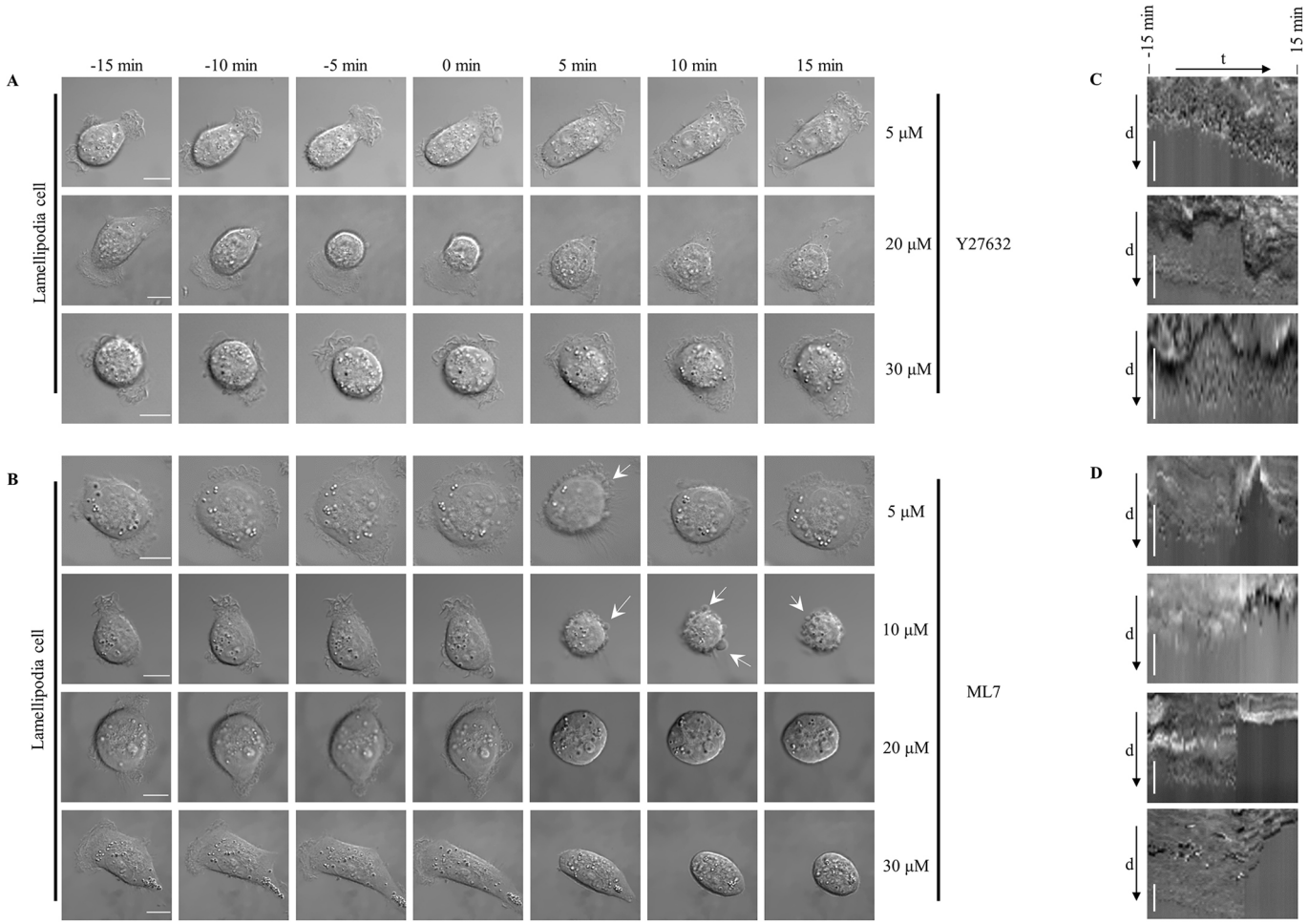

Fig. 3. Lamellipodia to blebbing conversion depends on MLCK activity. (A,B) Time-lapse images of lamellipodial cells in the presence of Y27632 (A) or ML7 (B) at the indicated concentrations. Images were captured for 15 min before and after the addition of inhibitors. Note that lamellipodial cells were converted to blebbing (arrows) within 5 min in the presence of 5–10 µM ML7, but stopped at >20 µM ML7. (C,D) The kymographs of the corresponding Y27632-treated (C) and ML7-treated (D) lamellipodial cells. Note that ML7-treated cells show steady rearward movement of the lamellipodium membrane. $n \geq 20$ cells for each treatment from three independent experiments. Scale bars: 10 µm (A,B), 5 µm (C,D).

siRNAs (esiRNAs). Because MDA-MB-231 cells express both ROCK1 and ROCK2 isoforms, we used RNAi against both isoforms. Fig. S6A,B show that specific RNAi could inhibit the expression of ROCK1 by 60%, ROCK2 by 83% and MLCK by 86% compared with the effect of a non-specific RNAi, GFPesiRNA. We quantified the number of cells showing blebbing or lamellipodia at 72 h post RNAi treatment. Fig. S6C,D demonstrate that 98% of cells showed lamellipodia when ROCKs were knocked down, whereas 70% of cells showed blebs when MLCK was knocked down, compared with GFPesiRNA-treated cells, which showed 26% blebbing and 74% lamellipodia.

Blebbing and lamellipodial cells were stained for RLC (red) and pRLC (green) following drug or esiRNA treatment, and images were captured using super-resolution confocal microscopy. Fig. 5A–D show that in control cells treated with neither drugs nor siRNA, both pRLC and RLC were present in blebs (Fig. 5A,C, i), whereas only pRLC was predominantly present in lamellipodia (Fig. 5B,D, i), suggesting that blebs contain both folded and unfolded forms of NMII and that lamellipodia contain mainly unfolded NMII forms. Line-scanning profiling at two different positions showed that blebbing cells were able to maintain a pRLC/RLC ratio greater than one at cell cortices when MLCK was inhibited (Fig. 5A,C, ii) or knocked down (Fig. 5A,C, iii). Similarly, lamellipodial cells were able to maintain pRLC/RLC ratio greater than one at lamellipodia when ROCK was inhibited (Fig. 5B,D, ii) or knocked down (Fig. 5B,D, iii). Note that the width of the region with pRLC/RLC ratio greater than one at lamellipodia was restricted to the edge of the cell in ROCK esiRNA- or Y27632-treated cells, whereas it was widely distributed over the lamellipodial region in control cells treated with neither drug nor esiRNA. Taken together with Fig. 4, these results suggest that MLCK-mediated RLC phosphorylation of NMII in ROCK esiRNA- or Y27632-treated cells may lead to the formation of slow contractile units of actomyosin complex, which stabilize lamellipodia. On the other hand, ROCK-mediated RLC phosphorylation of NMII in MLCK esiRNA- or ML7-treated cells may lead to the formation of faster contractile units of actomyosin complex, whose contractility initiates membrane detachment from the cortex and bleb retraction.

Blebbing and lamellipodia membranes possess different lipid order

NMIIs have been shown to be associated with anionic phospholipids of the plasma membrane, and NMII monomers can localize near the plasma membrane of lamellipodia and the cortex of blebs (Dey et al., 2017; Shutova et al., 2014; Li et al.,

Journal of Cell Science (2021) 134, jcs248732. doi:10.1242/jcs.248732

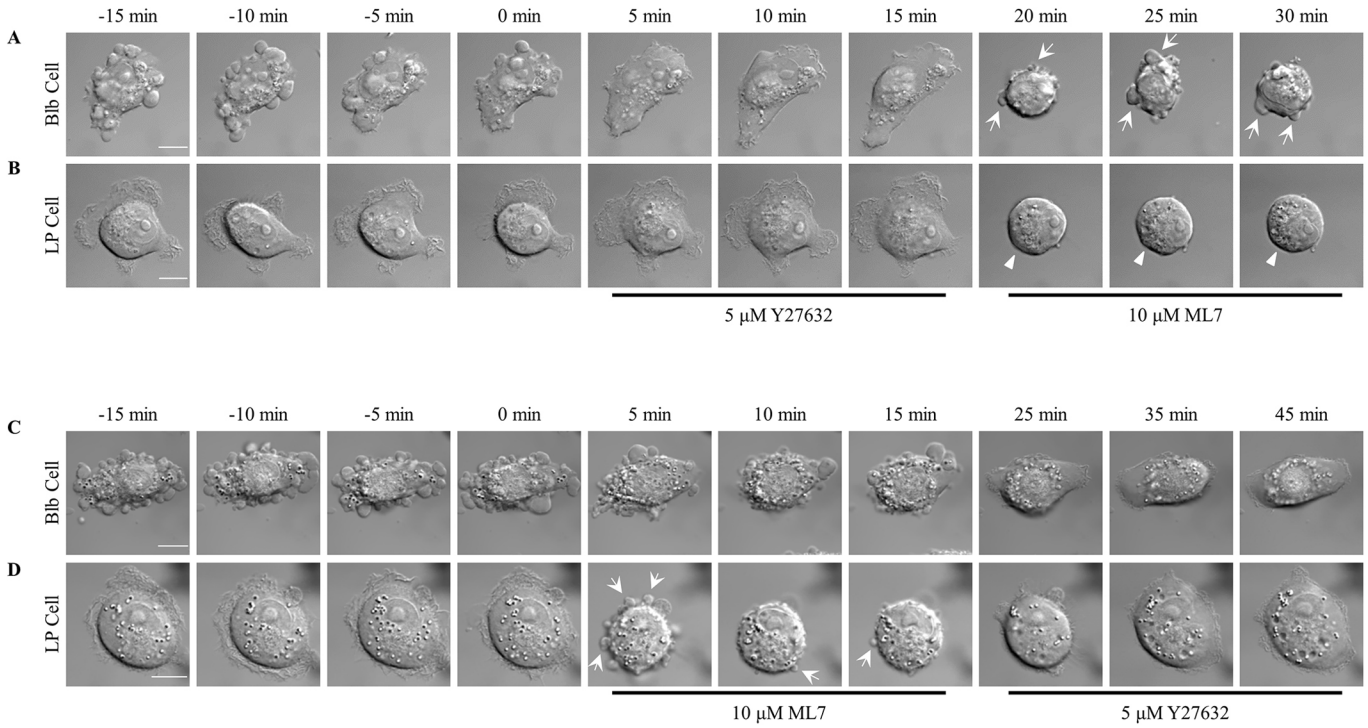

Fig. 4. ROCK and MLCK are interlinked in BLC and LBC. (A–D) Snapshots of the time-lapse movie of blebbing (A,C) and lamellipodial (B,D) cells treated with 5 µM Y27632 followed by 10 µM ML7 (A,B), or 10 µM ML7 followed by 5 µM Y27632 (C,D) at the indicated times. Note that Y27632 induces MLCK activity (A,B), whereas ML7 induces ROCK activity (C,D). Arrows and arrowheads indicate the appearance of blebs and no protrusion, respectively. $n \geq 20$ cells for each treatment from three independent experiments. Blb, blebbing; LP, lamellipodia. Scale bars: 10 µm.

1994; Liu et al., 2016). We wanted to evaluate whether membrane lipid order is different between blebbing and lamellipodia membranes and whether this can be associated with the activity of NMII. To assess the cell membrane lipid properties in blebbing and lamellipodia membranes, we performed quantitative imaging of lipid order in live-cell membranes using a polarity-sensitive probe, Laurdan, and two-photon microscopy. Ordered (peak emission ∼440 nm) and disordered fluid membrane regions (peak emission ∼490 nm) were visualized using a ratiometric measure of two emission regions known as generalized polarization, GP (see Materials and Methods, Eqn 1) (Sezgin et al., 2017). Because Laurdan can also internalize and stain intracellular membranes, we used a spectral imaging toolbox to remove cytosolic contribution of the internalized dyes and segmented the images using a plasma membrane segmentation module (Aron et al., 2017). The global GP histogram of MDA-MB 231 cellular membranes displayed a bimodal distribution centred at distinct GP values (C1=−0.15, and C2=0.25), indicative of co-existing fluid and ordered membrane regions in lamellipodia. Similarly, the global distribution for blebbing cells had GP values centred at C1=−0.17 and C2=0.25 (Fig. 6A,B). Upon comparing the plasma membrane regions, increased plasma membrane GP values were clearly visible for lamellipodia structures compared to blebs. Thus, this implies that increased lipid ordering may be associated with the transition from blebbing to lamellipodia in plasma membranes (Fig. 6D). This was also evident from increased surface coverage by the ordered lipid domains on the cell membrane (Fig. 6C). Taken together, these studies suggest that bleb membranes have less lipid order (and higher hydration at the lipid interfacial region) compared with that of lamellipodia membranes. This most likely is due to differential lipid compositions of blebbing and lamellipodial membranes.

DISCUSSION

Migratory cells show membrane protrusive activities – blebbing and formation of lamellipodia – for effective migration in the neighbouring environment. They can switch from blebbing to lamellipodia and vice versa depending on the matrix rigidity and cell mechanics (Sahai and Marshall, 2003; Bergert et al., 2012). Here, we provide evidence that the level of NMII activity present in a cell can differentially determine membrane protrusive activities.

We examined cellular morphology after the partial inhibition of NMII, rather than complete inhibition, in normal breast cells and in breast cancer tumour and metastasic cells. All the cell types underwent BLC when NMII was partially inhibited by (−) blebbistatin, suggesting the involvement of NMII activity in migratory plasticity. Similarly, Chikina et al. (2019b) and our own experiments (Movie 36) have established that LBC can be enhanced by inhibiting the Arp2/3 complex in HT1080 fibrosarcoma and MDA-MB-231 cells, respectively, and Dey et al. (2017) have shown that altering the amount of NMII isoforms can also trigger such a transition in MCF7 breast cancer cells. Taken together, these reports support a notion that the cytoskeletal network machinery, such as that involved in actin polymerization and NMII activity, can change the migratory plasticity.

Oakes et al. (2018) have proposed that NMII is not needed for lamellipodia. On the other hand, the involvement of NMII in lamellipodia was very much explained by a well-studied steady-state model system, in which the actin network at the leading edge of a migrating cell is maintained by the balance between polymerization and depolymerization of actin filaments. Henson et al. (1999) have shown that in sea urchin coelomocytes, actin polymerization provides ‘push’ retrograde flow by the addition of actin subunits at the leading edge, whereas NMII acts as a ‘puppeteer’, pulling on actin strings. Similarly, in primary neurons,

Journal of Cell Science (2021) 134, jcs248732. doi:10.1242/jcs.248732

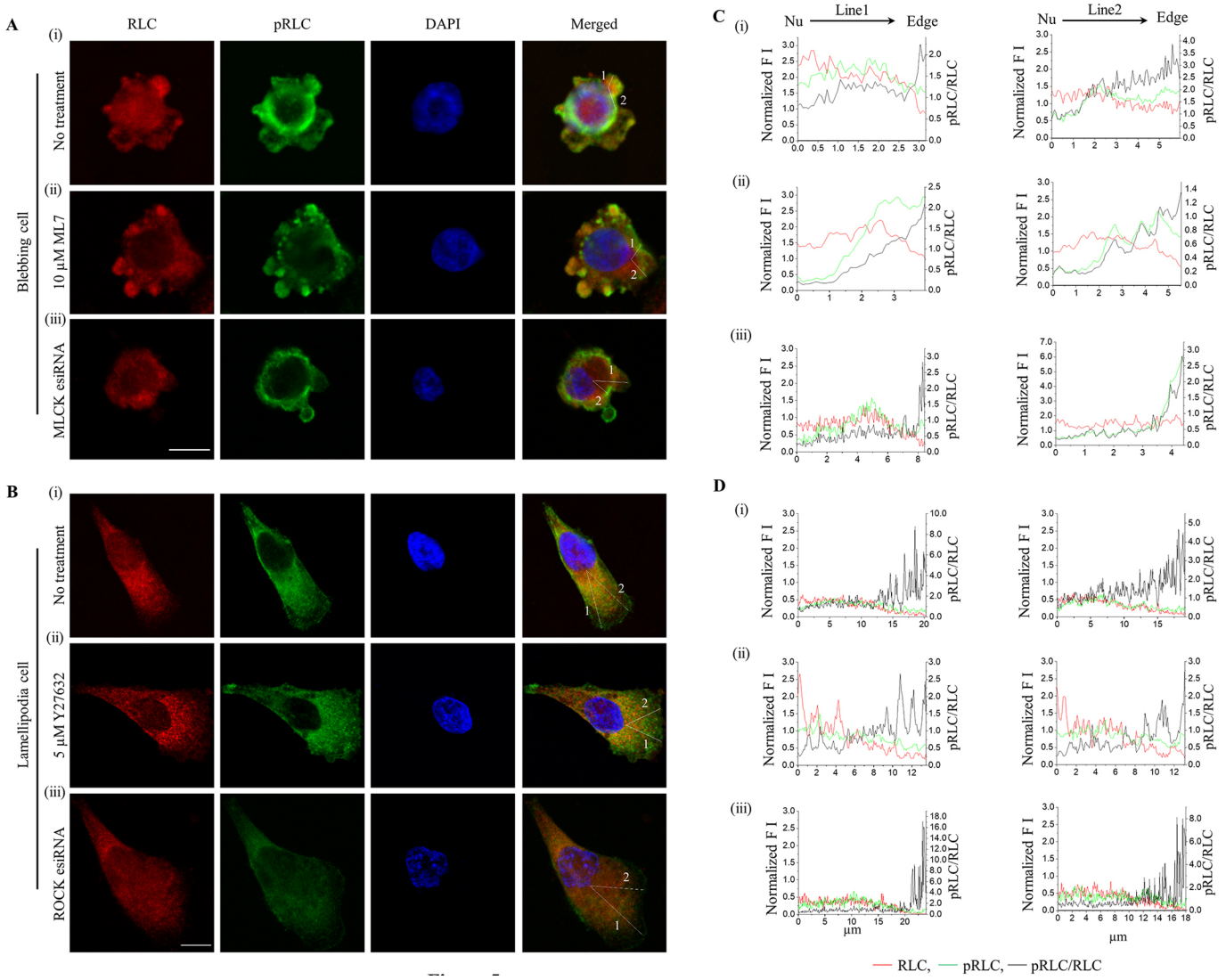

Fig. 5. Distinct phosphorylated RLC in blebbing versus lamellipodia membrane protrusion. (A,B) Representative confocal microscopy images of blebbing (A) and lamellipodial (B) MDA-MB-231 cells. Blebbing cells in the absence (A,i) or presence of ML-7 (A,ii) or MLCK esiRNA (A,iii) and lamellipodial cells in the absence (B,i) or presence of Y27632 (B,ii) or ROCK esiRNA (B,iii) were stained for pRLC (green), RLC (red) and nuclear DNA (DAPI, blue). Lines 1 and 2 indicate positions of the line scans shown in the corresponding graphs in C and D. (C,D) Line scans of pRLC and RLC fluorescence intensity from nucleus (Nu) to cell edge of both blebbing (C,i–iii) and lamellipodial cells (D,i–iii), treated as described in A and B. The fluorescence intensity at each point was normalized by considering the total fluorescence intensity of individual fluorophores across the line as 100%. Individual normalized fluorescence intensities of pRLC and RLC are shown on the left axis, whereas the pRLC:RLC ratio is shown on the right axis of the graph. The experiment was repeated three times. FI, fluorescence intensity. Scale bars: 10 µm.

retrograde actin flow works with cell adhesion, and its steady-state level is regulated by both NMII contractility and actin network treadmilling (Medeiros et al., 2006). Our data emphasizes that lower activity of NMII is needed for maintaining lamellipodial dynamics, based on the following findings: (1) at low concentration of (−) blebbistatin (2.5 µM), lamellipodia were not affected; and (2) lamellipodial protrusion stopped earlier than blebbing in the presence of a higher dose of (−) blebbistatin (10 µM; Fig. 1). Such low activity of NMII in lamellipodia may be controlled by MLCK, because formation of lamellipodia was stopped by ML7, but not by Y27632 (Fig. 6).

The question arises why the treatment of lamellipodial cells with a higher dose of ML7 generated complete roundedness, as compared to the appearance of finger-like structures that occurred in the presence of (−) blebbistatin. We hypothesize that the rounded morphology, which could be a consequence of loss of adhesion at the convergent zone, was due to a lack of availability of NMII filaments, which in turn is dependent on MLCK activity at the lamella. Shutova et al. (2014) have shown that the actin filaments are interspersed by NMII monomers whose activity is needed for focal complex formation at lamellipodia. Inhibition of NMII activity by (−) blebbistatin might subsequently prevent focal complex formation, which eventually could lead to the formation of finger-like structures. Interestingly, treatment with lower doses of ML7 caused transient appearance of blebbing in the lamellipodial cells (Movie 15). This transient blebbing was associated with LBC followed by immediate BLC. In both cases, we observed the quick appearance of similar finger-like structures, which could be due to further reduction of NMII activity and, consequently, the presence of fewer focal adhesions at the lamella of the lamellipodial cell.

Journal of Cell Science (2021) 134, jcs248732. doi:10.1242/jcs.248732

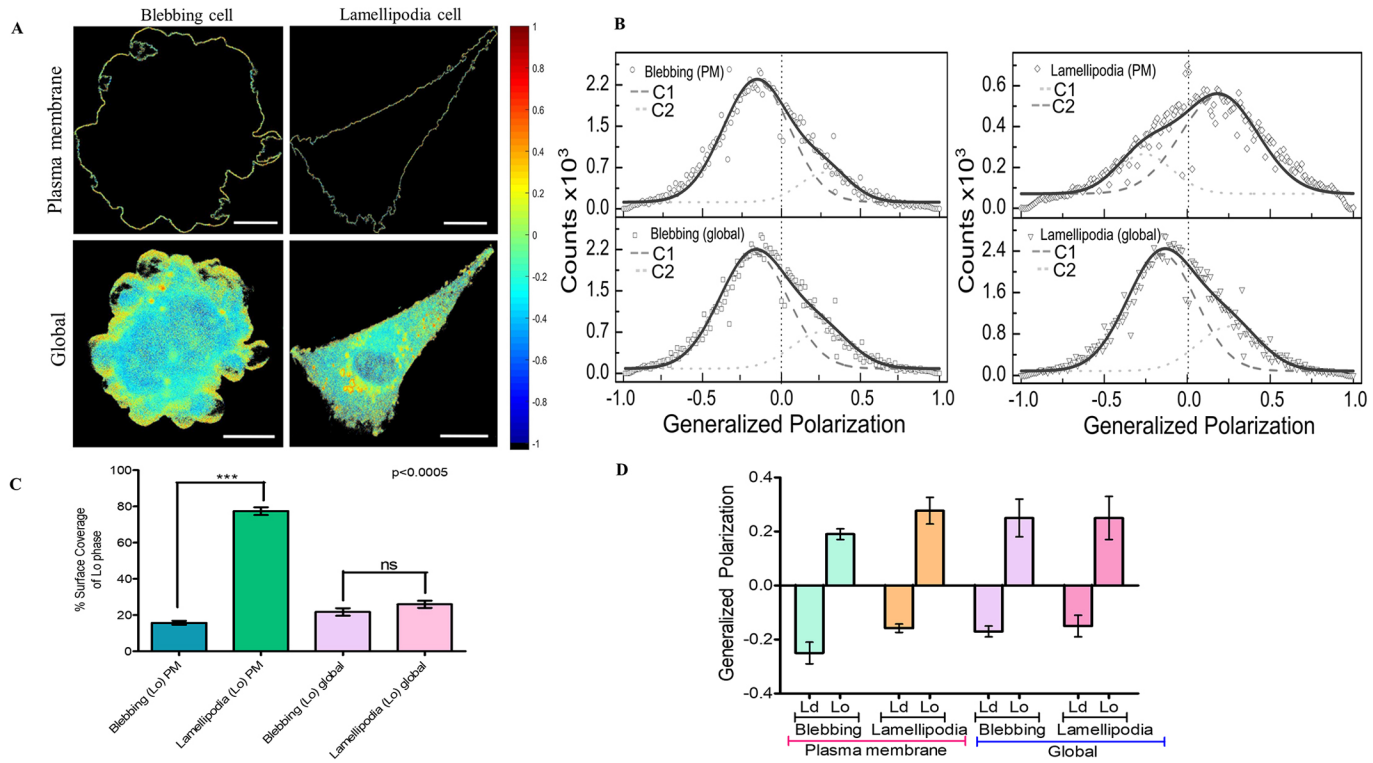

Fig. 6. Distinct lipid order in blebbing and lamellipodia membranes. (A) Pseudo-coloured images of global and plasma membrane GP values for blebbing and lamellipodial MDA-MB-231 cells. (B) Associated global and plasma membrane (PM) segmented GP distributions from the stack of GP images (n=50, N=3) and deconvolution by fitting two Gaussian distributions, C1 and C2. The C1 and C2 distributions denote the GP of the disordered lipid phase (Ld) and the ordered lipid phase (Lo), respectively. (C) Percentage of surface coverage of Lo phase distributed in normalized GP distribution expressed as the area under the curve of two Gaussian distributions. Data are mean±s.e.m. from three independent experiments. ***P<0.0005; ns, not significant (unpaired, two-tailed Student's t-test). (D) Lipid order and fluidity (generalized polarization) of the cellular membrane. Data are mean±s.e.m. from three independent experiments. Scale bars: 10 µm.

With our current experimental setup, we could not study the dynamics of such short-lived finger-like structures during LBC and BLC. Further study is needed to understand the importance of such membrane activities during migratory plasticity.

We cannot rule out the possibility of a role for adhesion complexes in regulating NMII activity during the conversion. NMII contractility modulates integrin signalling and affects the composition and function of focal adhesions (Kuo et al., 2011). Knockdown of integrin β1 resulted in an increase in the percentage of cells with a blebbing phenotype (Fig. S6E–G). Deakin and Turner (2011) established that the focal adhesion adaptor proteins Paxillin and Hic-5 (also known as TGFB1I1) control efficient mesenchymal and amoeboid invasion by regulating RhoGTPase signalling and NMII activity. Therefore, integrin or other signalling pathways may counterbalance NMII activity during the conversion, which needs to be further investigated.

We treated MDA-MB-231 cells with (−) blebbistatin at lower doses and found that at IC_{50} concentration (~2 µM, at which NMII is inhibited by 50%), blebbing cells converted into lamellipodial cells, suggesting that dynamics of NMII in blebbing cells (amoeboid) is different to that in lamellipodial cells (mesenchymal mode). Blebbing and lamellipodial cells showed differential conversion when they were treated with Y27632 followed by ML7 (Fig. 4). Blebbing cells formed lamellipodia in the presence of Y27632 but returned to blebbing when ML7 was subsequently added, whereas lamellipodial cells adopted a rounded phenotype instead of blebbing in the presence of ML7. These responses were possibly due to MLCK and ROCK activities being interconnected during the conversions. The differential levels of contractility guided by different NMII activity in blebbing and lamellipodial cells were also reflected by the values of two time constants correlated with contractility, τ_1 and τ_2, for those membrane protrusions (Sen and Kumar, 2009) (Fig. S7A–C). These findings suggest that even a single cell line can maintain heterogeneity in the context of NMII activity and membrane protrusive activities.

We also correlated NMII-dependent membrane protrusive activities with membrane lipid order in the blebbing and lamellipodial membranes of MCF7 and MCF10A cells (Fig. S8), and compared this with findings from MDA-MB-231 cells (Fig. 6). We found that the plasma membranes of blebbing MCF7 and MCF10A cells in the PM segmentation mode had a bimodal GP distribution centred at C1=−0.05 and C2=0.54 for MCF7, and at C1=−0.12 and C2=0.41 for MCF10A (Fig. S8). The global bimodal GP pattern remained almost the same for both lamellipodial and blebbing membranes in MCF7 cells [centred at C1=−0.08 and C2=0.29 (lamellipodia) and 0.36 (blebs)] and MCF10A cells [centred at C1=−0.24 and C2=0.14 (lamellipodia) and 0.11 (blebs)]; however, the membranes varied in surface abundance of the ordered lipid domains. Surprisingly, lamellipodial plasma membrane in MCF7 and MCF10A cells was associated with decreasing membrane lipid order (and also with decreased surface coverage by ordered domains), in contrast to that observed with MDA-MB-231 cells. Further study is warranted to decipher whether lipid order can be associated with NMII activity or membrane protrusive activities such as blebs, filopodia and lamellipodia in human diseases (Beloribi-Djefaflia et al., 2016; Honigmann et al., 2014; Moon et al., 2017; Sezgin et al., 2017), because these are considered as buffer systems for the plasma membrane (Gauthier et al., 2012).

Journal of Cell Science (2021) 134, jcs248732. doi:10.1242/jcs.248732

We observed that amount of NMII activity needed for blebbing or formation of lamellipodia was different in a variety of cell lines, because the inhibitor concentration required to induce conversion or stop protrusion was not the same (Figs 1–3; Figs S2–S5). This prompted us to hypothesize that the ability of binding partners to bind with NMII depends on the activity of NMII, which is in turn dependent on the cellular context. How NMII activity is regulated or how effector molecules assemble upon sensing the degree of NMII activity during BLC and LBC needs to be further investigated. Jiao et al. (2018) have established that ezrin–MYOGEF (myosin II-interacting guanine-nucleotide-exchange factor, also known as PLEKHG6) interaction is needed for the recruitment of MYOGEF to the bleb membrane in order to activate RhoA for bleb retraction, suggesting the involvement of NMII in the bleb life cycle, which may be controlled by signals close to the plasma membrane (Wu et al., 2009).

The switching between protrusion types and motility modes, which needs to be rapid in order to adapt to the altered environment, has been proposed to facilitate cancer cell dissemination (Bergert et al., 2012). This may be further supported by our observation, where 60% of blebbing cells showed BLC within 15 min under serum-starved conditions (Fig. S7D–F, Movies 37,38). The inherent conversion ability of cells could indeed allow selection of the most efficient migration mode in complex environments, such as those with heterogeneous availability of nutrients and rigidity of the matrix (Petrie and Yamada, 2012; Sanz-Moreno and Marshall, 2010; Friedl, 2004). This also brings to the forefront the role of lipid composition (or lipid order) and membrane properties in driving facile switching between the two phenotypes.

Note that (1) lamellipodial cells were able to show LBC in the presence of 10 µM ML7, followed by BLC when ML7 was removed (Movie 26); (2) blebbing cells were able to show BLC in the presence of 2.5 µM (−) blebbistatin, followed by LBC when 2.5 µM (−) blebbistatin was removed (Movie 7); (3) MLCK esiRNA caused increased expression of ROCK2 (Fig. S6A); and (4) ROCK inhibition did not stop the activity lamellipodia (Fig. 3A). Taken together, these observations lead us to hypothesize that cellular plasticity mainly depends on NMII motor activity and assembly into filaments (a prerequisite for building actomyosin contractile units; Titus, 2017), which are mainly controlled by MLCK, and that ROCK may further activate NMII to increase NMII motor activity and filament assembly, resulting in the blebbing phenotype. Kassianidou et al. (2017) and Titus (2017) have proposed that

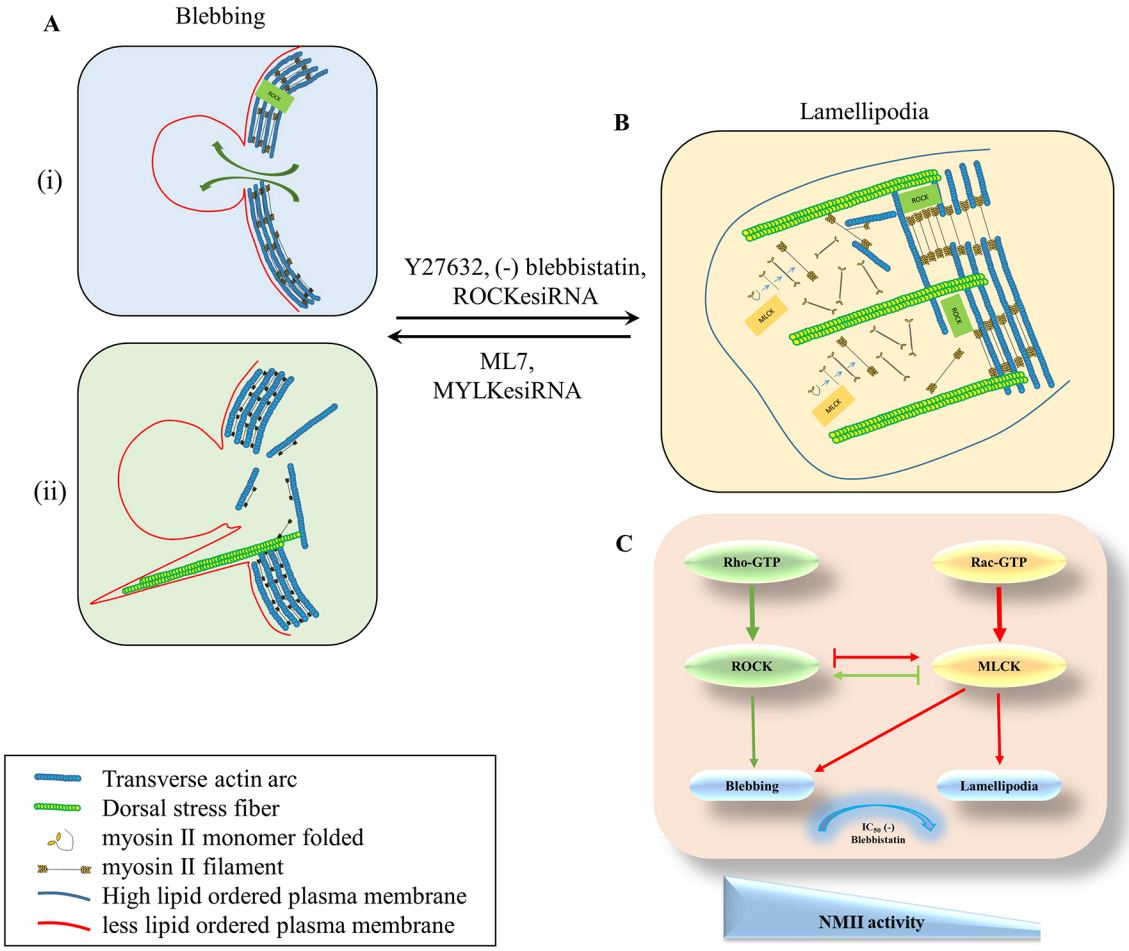

Fig. 7. Model of NMII activity and filament formation with membrane protrusive activity. (A) Schematic diagrams of bleb formation at positions where (i) the plasma membrane is detached from the cortex due to higher actomyosin contractility and flow of cytosol (arrows), or (ii) the cytoskeleton network is more sparse around the filopodial root. (B) Schematic diagram of lamellipodium actin filaments with myosin monomers just underneath the plasma membrane and NMII filaments at the interior. NMII monomers at the lamellipodium undergo NMII nucleation and form filaments, which then stack and stabilize actin bundles at the interior. NMII nucleation is associated with MLCK-mediated RLC phosphorylation. (C) Schematic diagram of the degree of NMII activity versus membrane protrusive activity. NMII activity can be regulated by both MLCK and ROCK, which are interlinked during BLC and LBC.

ROCK activity is higher at the centre of cells, whereas MLCK activity is higher at the periphery of cells. Further study is needed to separate blebbing and lamellipodial cells to understand the differences in the degree of MLCK and ROCK activity and the consequent NMII activity in cells. We hypothesize a model (Fig. 7) in which migratory plasticity may be governed by the abundance of different NMII species, including folded and compact monomers, dimers and tetramers, and the degree of filament-forming property at different locations between the cell edge and interior (Shutova et al., 2014; Beach et al., 2017). Understanding the regulatory mechanism of NMII dynamics in migratory plasticity may facilitate the design of therapeutic approaches to combat diseases that are associated with cellular migration.

MATERIALS AND METHODS

Cell culture

MDA-MB-231, MCF7, and MCF10A cells were obtained from American Type Culture Collection (ATCC, Virginia, USA), and maintained as per their guidelines. The MDA-MB-231 cell line was grown in growth medium (GM): Leibovitz L-15 medium containing 10% fetal bovine serum and 1% penicillin-streptomycin (Thermo Fisher Scientific, MA, USA) in a 37°C incubator without CO_2, as per ATCC guidelines. The MCF7 cell line was grown in GM: Dulbecco's modified Eagle's medium (Thermo Fisher Scientific) containing 10% fetal bovine serum, 1% penicillin-streptomycin and 0.1% insulin in a 5% CO_2 incubator at 37°C. GM for MCF10A cells was DMEM/F12 supplemented with 5% horse serum, 20 ng/ml epidermal growth factor, 100 ng/ml cholera toxin, 0.01 mg/ml insulin and 500 ng/ml hydrocortisone (Sigma-Aldrich, MO, USA) in a 5% CO_2 incubator at 37°C, as per ATCC guidelines.

Inhibitors and esiRNA

The inhibitors Y27632, ML7, TBBt, and (−) blebbistatin were purchased from Sigma-Aldrich, TG100-115 was purchased from Santa Cruz Biotechnology (TX, USA), and Go 6976 and (+) blebbistatin were purchased from Tocris bioscience (Bristol, UK). Laurdan was purchased from Sigma-Aldrich. Cells were treated with 0–50 µM inhibitors for 15–30 min, and 0.2% DMSO was used as control. For RNAi experiments, 10^5 MDA-MB-231 cells were transfected with 4 nM esiRNA or 50 nM siRNA using Lipofectamine RNAimax (ThermoFisher) according to the manufacturer's protocol. EsiRNAs against MYLK (EHU158801, referring to transcript variant 3A, mRNA), ROCK1 (EHU034701), and ROCK2 (EHU030131) and GFP (EHUEGFP) were procured from Sigma-Aldrich. EsiRNA against GFP was used as a control for RNAi experiments (Keller et al., 2012; Chikina et al., 2019a). The siRNAs against integrin β1, and Universal Negative Control 1 tagged with Cyanine 3 (NS siRNA, #SIC003) were purchased from Sigma-Aldrich. The siRNA sequences for integrin β1 were 5′-GUGAAGACAUGGACGCUUA-3′ and 5′-UAAGCGUCCAUG-UCUUCAC-3′. The cells were analysed 72 h after transfection.

Immunofluorescence confocal microscopy

To determine the level of phosphorylated RLC (active) relative to total NMII RLC, we carried out a two antibody-based staining method following a previously published procedure (Zhang et al., 2019). MDA-MB-231 cells, grown in chamber slides, were fixed with 4% paraformaldehyde in phosphate-buffered saline (PBS) for 15 min at room temperature and then permeabilized with 0.1% Triton X-100 for 10 min. Cells were incubated with 3% BSA for 60 min followed by antibodies against pRLC (1:200; ThermoFisher, # MA5-15163) and RLC (1:200; Abcam, #ab79935) at 4°C overnight (Halder et al., 2019; Fu et al., 2015; Orgaz et al., 2020). Mouse and rabbit secondary antibodies conjugated with Alexa Fluor 488 or 594 (ThermoFisher) were added for 60 min for detecting pRLC and RLC, respectively. DAPI was used to stain nuclei. Coverslips were mounted using Prolong gold antifade reagent (ThermoFisher). Images were captured using a Zeiss LSM880 confocal microscope (Zeiss, Germany) controlled by Zen Blue software. The ratio of intensity values of phosphorylated RLC to that of total NMII RLC in a given line scan was considered to determine the active NMII to total NMII RLC.

Time-lapse video microscopy

Time-lapse images of blebbing and lamellipodia in MDA-MB-231, MCF7 and MCF 10A cells were captured using a confocal laser-scanning Eclipse Ti-E microscope equipped with a plan apochromatic VC 60×/1.4 oil objective, and Digital Sight DS-Qi1MC monochromatic camera with NIS-AR software (Nikon, Tokyo, Japan) (Tinevez et al., 2009; Dey et al., 2017). The DIC images of blebbing or lamellipodial cells were captured at 20 s intervals for 30–75 min using 488 nm argon gas laser with 200 µW power in a stage incubator at 37°C supplied with or without 5% CO_2. Movies were prepared at 10 frames/s using NIS-AR software.

Laurdan general polarization imaging

MDA-MB-231 cells were incubated with 10 µM Laurdan for 3–4 h and washed with serum-free medium before imaging on a laser-scanning confocal microscope (Carl Zeiss, Germany) monitoring fluorescence emission of Laurdan using a 780 nm multi-photon laser excitation (Titanium sapphire, Coherent Radiation, CA) using 40× water objective. Emission was collected between 415 and 700 nm by a 32-channel GaAsP detector at ≈8.9 nm wavelength intervals. For the calculation of the generalized polarization (GP) values, a previously reported spectral imaging toolbox was employed (Aron et al., 2017; Owen et al., 2012). Spectral analysis was done with images of cells and segmented by lasso segmentation. The value of membrane segmentation in spectral analysis was highlighted by comparing the spectra and GP distributions of the segmented cells along with the pre-segmentation images. Pixel counts of each image were collected from the segmentation toolbox folders, based on Eqn 1, and were used to generate the pseudo-coloured GP maps, fluorescence spectra, and histograms.

$$\mathrm{GP} = \frac{I_{439} - I_{493}}{I_{439} + I_{493}} \quad (1)$$

GP distributions were obtained from the histogram of the GP images, which were fitted with either a single or double peak Gaussian functions using Origin Software (Origin Pro.9.1). GP values were displayed in a range of −1.0 (high fluidity) to +1.0 (lowest fluidity, ordered phase) using a custom colour palette.

Kymographs

Kymographs were generated using ImageJ (NIH, MD, USA) software by taking 1 pixel wide rectangular regions in the direction of edge movement.

De-adhesion assay

De-adhesion assay experiment was carried out following previously published protocol (Sen and Kumar, 2009). Briefly, MDA-MB-231 cells were washed with PBS and treated with 0.25% trypsin EDTA (Sigma-Aldrich). Time-lapse images were captured at 10 s intervals until the cell became completely rounded. Cell contact area was measured at different time points using ImageJ software. The time-dependent normalized area ($A_{\mathrm{normalized}}$) was measured by dividing the difference between the cell area at time t (A_t) and at time t=0 (A_{initial}) using Eqn 2. The normalized area and time were fitted to a sigmoidal curve to obtain the time constants τ_1 and τ_2 from Boltzmann Eqn 3.

$$A_{\mathrm{normalized}} = \frac{A_{\mathrm{initial}} - A_t}{A_{\mathrm{initial}} - A_{\mathrm{final}}} \quad (2)$$

$$A_{\mathrm{normalized}} = \frac{1}{1 + e^{(t-\tau_1)/\tau_2}} \quad (3)$$

Immunoblotting

Cell lysates from integrin β1 siRNA-treated or nonspecific siRNA-treated MDA-MD-231 cells were fractionated by SDS-PAGE on an 8% polyacrylamide Tris-Glycine gel and transferred onto 0.45 µm polyvinylidene difluoride membrane (Millipore, USA). The membranes were blocked using 5% nonfat milk (Sigma-Aldrich) and 0.05% Tween-20, and incubated with primary antibody specific to integrin β1 (1:5000; BD Bioscience, #610467) or GAPDH (1:10,000; Sigma-Aldrich, #G8795) overnight at 4°C. The membranes were then washed and incubated with secondary antibody conjugated with horseradish peroxidase for 2 hours at

room temperature. Chemiluminescence signal was captured using a ChemiDoc Touch Imaging system (Bio-Rad, USA). The band intensity was quantified using ImageJ software (NIH, USA).

Reverse transcription PCR

Total RNA was isolated from ROCK1 and 2, MLCK or GFP esi RNA-treated MDA-MB-231 cells using the RNeasy Mini Kit (Qiagen, CA). 1 µg of total RNA was reverse transcribed using EvoScript Universal cDNA Master (Roche, Switzerland). The cDNA was amplified using primer sets specific for ROCK1 (forward primer, 5'-CTGGGGACAGTTTTGAGACT-3'; reverse primer, 5'- CACCTCTACCAATCACCTTC-3'), ROCK2 (forward primer, 5'-GTCAGGATGCAGATGGGCAA-3'; reverse primer, 5'-CAGCAATTGAACGAGCCAGT-3'), MLCK (forward primer, 5'-CTGGGTCACCGTCCATGAAA-3'; reverse primer, 5'-AAGGCTGTGCTGAGTTCCTC-3') and GAPDH (forward primer, 5'-GAGTCAACGGATTTGGTCGT-3'; reverse primer, 5'-TTGATTTTGGAGGGATCTCG-3') using Taq PCR Reaction Mix (Sigma-Aldrich). The PCR products were run on a 1.8% agarose gel and the band intensity was quantified using ImageJ software (NIH, USA).

Plasmid transfection

A total of $1x10^5$ MDA-MB-231 cells were transfected with 1 µg of plasmid DNA using Lipofectamine 2000 (Thermo Fisher Scientific, Waltham, MA) according to the manufacturer's protocol (Dey et al., 2017). LifeAct–GFP and PLC δ1–GFP plasmids were received from Hidde Ploegh (Whitehead Institute for Biomedical Research, Cambridge, MA) and Thomas Balla (NIH, USA), respectively, as gifts. GFP images were captured using a confocal laser scanning microscope (Nikon, Tokyo, Japan).

Serum starvation

MDA-MB-231 cells were grown in Leibovitz L-15 medium containing 10% fetal bovine serum and 1% penicillin-streptomycin (Thermo Fisher Scientific, MA, USA) in a 37°C incubator without CO_2, as per ATCC guidelines. Growth medium was replaced with medium containing no serum, and time-lapse images of blebbing and lamellipodial cells were captured using time-lapse video microscopy (Nikon) for 15 min at 20 s intervals.

Acknowledgements

We thank Hidde Ploegh (Whitehead Institute for Biomedical Research, Cambridge, MA) and Thomas Balla (NIH, USA) for providing us with LifeAct–GFP and PLC δ1–GFP plasmids, respectively. We acknowledge Raja Paul and Debdatta Halder (IACS), Aswin T. Srivatsav (IIT Bombay), Sumit K Dey (IFOM – the FIRC institutes of Molecular Oncology, Italy) and Bidisha Sinha (IISER-Kolkata) for their technical support and help. We thank all other laboratory members for reading the manuscript and providing valuable comments. We thank the Technical Research Center, IACS for use of a super-resolution microscope.

Competing interests

The authors declare no competing or financial interests.

Author contributions

Conceptualization: I.G., S.S.J.; Methodology: I.G., R.K.S., M.M., S.S.J.; Software: I.G., S.K., S.S.J.; Validation: I.G., R.K.S., S.K., S.S.J.; Formal analysis: I.G., S.S.J.; Investigation: I.G., R.K.S., M.M., S.K., S.S.J.; Resources: S.S.J.; Data curation: I.G., S.S.J.; Writing - original draft: I.G., M.M., S.S.J.; Writing - review & editing: I.G., R.K.S., M.M., S.K., S.S.J.; Visualization: I.G., S.S.J.; Supervision: S.S.J.; Project administration: S.S.J.; Funding acquisition: S.S.J.

Funding

We thank the Council of Scientific and Industrial Research, India for a fellowship to I.G. This work was supported by the Department of Science and Technology, Ministry of Science and Technology, India (EMR/2015/002054 to S.S.J.) and IACS.

Supplementary information

Supplementary information available online at
https://jcs.biologists.org/lookup/doi/10.1242/jcs.248732.supplemental

References

Aman, A. and Piotrowski, T. (2010). Cell migration during morphogenesis. *Dev. Biol.* **341**, 20-33. doi:10.1016/j.ydbio.2009.11.014

Aron, M., Browning, R., Carugo, D., Sezgin, E., Bernardino de la Serna, J., Eggeling, C. and Stride, E. (2017). Spectral imaging toolbox: segmentation, hyperstack reconstruction, and batch processing of spectral images for the determination of cell and model membrane lipid order. *BMC Bioinformatics* **18**, 254. doi:10.1186/s12859-017-1656-2

Barry, D. J., Durkin, C. H., Abella, J. V. and Way, M. (2015). Open source software for quantification of cell migration, protrusions, and fluorescence intensities. *J. Cell Biol.* **209**, 163-180. doi:10.1083/jcb.201501081

Beach, J. R., Bruun, K. S., Shao, L., Li, D., Swider, Z., Remmert, K., Zhang, Y., Conti, M. A., Adelstein, R. S., Rusan, N. M. et al. (2017). Actin dynamics and competition for myosin monomer govern the sequential amplification of myosin filaments. *Nat. Cell Biol.* **19**, 85-93. doi:10.1038/ncb3463

Beloribi-Djefaflia, S., Vasseur, S. and Guillaumond, F. (2016). Lipid metabolic reprogramming in cancer cells. *Oncogenesis* **5**, e189. doi:10.1038/oncsis.2015.49

Berg, J. S., Powell, B. C. and Cheney, R. E. (2001). A millennial myosin census. *Mol. Biol. Cell* **12**, 780-794. doi:10.1091/mbc.12.4.780

Bergert, M., Chandradoss, S. D., Desai, R. A. and Paluch, E. (2012). Cell mechanics control rapid transitions between blebs and lamellipodia during migration. *Proc. Natl. Acad. Sci. USA* **109**, 14434-14439. doi:10.1073/pnas.1207968109

Caswell, P. T. and Zech, T. (2018). Actin-based cell protrusion in a 3D matrix. *Trends Cell Biol.* **28**, 823-834. doi:10.1016/j.tcb.2018.06.003

Charras, G. T., Hu, C.-K., Coughlin, M. and Mitchison, T. J. (2006). Reassembly of contractile actin cortex in cell blebs. *J. Cell Biol.* **175**, 477-490. doi:10.1083/jcb.200602085

Chikina, A. S., Rubtsova, S. N., Lomakina, M. E., Potashnikova, D. M., Vorobjev, I. A. and Alexandrova, A. Y. (2019a). Transition from mesenchymal to bleb-based motility is predominantly exhibited by CD133-positive subpopulation of fibrosarcoma cells. *Biol. Cell* **111**, 245-261. doi:10.1111/boc.201800078

Chikina, A. S., Svitkina, T. M. and Alexandrova, A. Y. (2019b). Time-resolved ultrastructure of the cortical actin cytoskeleton in dynamic membrane blebs. *J. Cell Biol.* **218**, 445-454. doi:10.1083/jcb.201806075

Coluccio, L. M. (2007). *Myosins: A Superfamily of Molecular Motors*. Springer Science & Business Media.

Deakin, N. O. and Turner, C. E. (2011). Distinct roles for paxillin and Hic-5 in regulating breast cancer cell morphology, invasion, and metastasis. *Mol. Biol. Cell* **22**, 327-341. doi:10.1091/mbc.e10-09-0790

Dey, S. K., Singh, R. K., Chattoraj, S., Saha, S., Das, A., Bhattacharyya, K., Sengupta, K., Sen, S. and Jana, S. S. (2017). Differential role of nonmuscle myosin II isoforms during blebbing of MCF-7 cells. *Mol. Biol. Cell* **28**, 1034-1042. doi:10.1091/mbc.e16-07-0524

Dupré, L., Houmadi, R., Tang, C. and REY-Barroso, J. (2015). T lymphocyte migration: an action movie starring the actin and associated actors. *Front. Immunol.* **6**, 586. doi:10.3389/fimmu.2015.00586

Friedl, P. (2004). Prespecification and plasticity: shifting mechanisms of cell migration. *Curr. Opin. Cell Biol.* **16**, 14-23. doi:10.1016/j.ceb.2003.11.001

Fu, Y., Huang, C., Xu, X., Gu, H., Ye, Y., Jiang, C., Qiu, Z. and Xie, X. (2015). Direct reprogramming of mouse fibroblasts into cardiomyocytes with chemical cocktails. *Cell Res.* **25**, 1013-1024. doi:10.1038/cr.2015.99

Gauthier, N. C., Masters, T. A. and Sheetz, M. P. (2012). Mechanical feedback between membrane tension and dynamics. *Trends Cell Biol.* **22**, 527-535. doi:10.1016/j.tcb.2012.07.005

Giannone, G., Dubin-Thaler, B. J., Döbereiner, H.-G., Kieffer, N., Bresnick, A. R. and Sheetz, M. P. (2004). Periodic lamellipodial contractions correlate with rearward actin waves. *Cell* **116**, 431-443. doi:10.1016/S0092-8674(04)00058-3

Giannone, G., Dubin-Thaler, B. J., Rossier, O., Cai, Y., Chaga, O., Jiang, G., Beaver, W., Döbereiner, H.-G., Freund, Y., Borisy, G. et al. (2007). Lamellipodial actin mechanically links myosin activity with adhesion-site formation. *Cell* **128**, 561-575. doi:10.1016/j.cell.2006.12.039

Golomb, E., Ma, X., Jana, S. S., Preston, Y. A., Kawamoto, S., Shoham, N. G., Goldin, E., Conti, M. A., Sellers, J. R. and Adelstein, R. S. (2004). Identification and characterization of nonmuscle myosin II-C, a new member of the myosin II family. *J. Biol. Chem.* **279**, 2800-2808. doi:10.1074/jbc.M309981200

Halder, D., Saha, S., Singh, R. K., Ghosh, I., Mallick, D., Dey, S. K., Ghosh, A., Das, B. B., Ghosh, S. and Jana, S. S. (2019). Nonmuscle myosin IIA and IIB differentially modulate migration and alter gene expression in primary mouse tumorigenic cells. *Mol. Biol. Cell* **30**, 1463-1476. doi:10.1091/mbc.E18-12-0790

Henson, J. H., Svitkina, T. M., Burns, A. R., Hughes, H. E., Macpartland, K. J., Nazarian, R. and Borisy, G. G. (1999). Two components of actin-based retrograde flow in sea urchin coelomocytes. *Mol. Biol. Cell* **10**, 4075-4090. doi:10.1091/mbc.10.12.4075

Honigmann, A., Mueller, V., Ta, H., Schoenle, A., Sezgin, E., Hell, S. W. and Eggeling, C. (2014). Scanning STED-FCS reveals spatiotemporal heterogeneity of lipid interaction in the plasma membrane of living cells. *Nat. Commun.* **5**, 5412. doi:10.1038/ncomms6412

Jiao, M., Wu, D. and Wei, Q. (2018). Myosin II-interacting guanine nucleotide exchange factor promotes bleb retraction via stimulating cortex reassembly at the bleb membrane. *Mol. Biol. Cell* **29**, 643-656. doi:10.1091/mbc.E17-10-0579

Kassianidou, E., Hughes, J. H. and Kumar, S. (2017). Activation of ROCK and MLCK tunes regional stress fiber formation and mechanics via preferential myosin

light chain phosphorylation. *Mol. Biol. Cell* **28**, 3832-3843. doi:10.1091/mbc.e17-06-0401

Kazakova, O. A., Khapchaev, A. Y. and Shirinsky, V. P. (2020). MLCK and ROCK mutualism in endothelial barrier dysfunction. *Biochimie* **168**, 83-91. doi:10.1016/j.biochi.2019.10.010

Keller, C., Kroening, S., Zuehlke, J., Kunath, F., Krueger, B. and GOPPELT-Struebe, M. (2012). Distinct mesenchymal alterations in N-cadherin and E-cadherin positive primary renal epithelial cells. *PLoS ONE* **7**, e43584. doi:10.1371/journal.pone.0043584

Krummel, M. F., Friedman, R. S. and Jacobelli, J. (2014). Modes and mechanisms of T cell motility: roles for confinement and Myosin-IIA. *Curr. Opin. Cell Biol.* **30**, 9-16. doi:10.1016/j.ceb.2014.05.003

Kuo, J. C., Han, X., Hsiao, C. T., Yates, J. R., III and Waterman, C. M. (2011). Analysis of the myosin-II-responsive focal adhesion proteome reveals a role for β-Pix in negative regulation of focal adhesion maturation. *Nat. Cell Biol.* **13**, 383-393. doi:10.1038/ncb2216

Li, D., Miller, M. and Chantler, P. D. (1994). Association of a cellular myosin II with anionic phospholipids and the neuronal plasma membrane. *Proc. Natl. Acad. Sci. USA* **91**, 853-857. doi:10.1073/pnas.91.3.853

Liu, X., Shu, S., Billington, N., Williamson, C. D., Yu, S., Brzeska, H., Donaldson, J. G., Sellers, J. R. and Korn, E. D. (2016). Mammalian nonmuscle myosin II binds to anionic phospholipids with concomitant dissociation of the regulatory light chain. *J. Biol. Chem.* **291**, 24828-24837. doi:10.1074/jbc.M116.739185

Medeiros, N. A., Burnette, D. T. and Forscher, P. (2006). Myosin II functions in actin-bundle turnover in neuronal growth cones. *Nat. Cell Biol.* **8**, 215-226. doi:10.1038/ncb1367

Moon, S., Yan, R., Kenny, S. J., Shyu, Y., Xiang, L., Li, W. and Xu, K. (2017). Spectrally resolved, functional super-resolution microscopy reveals nanoscale compositional heterogeneity in live-cell membranes. *J. Am. Chem. Soc.* **139**, 10944-10947. doi:10.1021/jacs.7b03846

Oakes, P. W., Bidone, T. C., Beckham, Y., Skeeters, A. V., Ramirez-San Juan, G. R., Winter, S. P., Voth, G. A. and Gardel, M. L. (2018). Lamellipodium is a myosin-independent mechanosensor. *Proc. Natl. Acad. Sci. USA* **115**, 2646-2651. doi:10.1073/pnas.1715869115

Orgaz, J. L., Crosas-Molist, E., Sadok, A., Perdrix-Rosell, A., Maiques, O., Rodriguez-Hernandez, I., Monger, J., Mele, S., Georgouli, M., Bridgeman, V. et al. (2020). Myosin II reactivation and cytoskeletal remodeling as a hallmark and a vulnerability in melanoma therapy resistance. *Cancer Cell* **37**, 85-103.e9. doi:10.1016/j.ccell.2019.12.003

Owen, D. M., Rentero, C., Magenau, A., Abu-Siniyeh, A. and Gaus, K. (2012). Quantitative imaging of membrane lipid order in cells and organisms. *Nat. Protoc.* **7**, 24-35. doi:10.1038/nprot.2011.419

Palamidessi, A., Frittoli, E., Garré, M., Faretta, M., Mione, M., Testa, I., Diaspro, A., Lanzetti, L., Scita, G. and Di Fiore, P. P. (2008). Endocytic trafficking of Rac is required for the spatial restriction of signaling in cell migration. *Cell* **134**, 135-147. doi:10.1016/j.cell.2008.05.034

Paluch, E. K. and Raz, E. (2013). The role and regulation of blebs in cell migration. *Curr. Opin. Cell Biol.* **25**, 582-590. doi:10.1016/j.ceb.2013.05.005

Petrie, R. J. and Yamada, K. M. (2012). At the leading edge of three-dimensional cell migration. *J. Cell Sci.* **125**, 5917-5926. doi:10.1242/jcs.093732

Ponti, A., Machacek, M., Gupton, S. L., Waterman-Storer, C. M. and Danuser, G. (2004). Two distinct actin networks drive the protrusion of migrating cells. *Science* **305**, 1782-1786. doi:10.1126/science.1100533

Reig, G., Pulgar, E. and Concha, M. L. (2014). Cell migration: from tissue culture to embryos. *Development* **141**, 1999-2013. doi:10.1242/dev.101451

Sahai, E. and Marshall, C. J. (2003). Differing modes of tumour cell invasion have distinct requirements for Rho/ROCK signalling and extracellular proteolysis. *Nat. Cell Biol.* **5**, 711-719. doi:10.1038/ncb1019

Sanz-Moreno, V. and Marshall, C. J. (2010). The plasticity of cytoskeletal dynamics underlying neoplastic cell migration. *Curr. Opin. Cell Biol.* **22**, 690-696. doi:10.1016/j.ceb.2010.08.020

Sanz-Moreno, V., Gadea, G., Ahn, J., Paterson, H., Marra, P., Pinner, S., Sahai, E. and Marshall, C. J. (2008). Rac activation and inactivation control plasticity of tumor cell movement. *Cell* **135**, 510-523. doi:10.1016/j.cell.2008.09.043

Sen, S. and Kumar, S. (2009). Cell-matrix de-adhesion dynamics reflect contractile mechanics. *Cell Mol. Bioeng.* **2**, 218-230. doi:10.1007/s12195-009-0057-7

Sezgin, E., Levental, I., Mayor, S. and Eggeling, C. (2017). The mystery of membrane organization: composition, regulation and roles of lipid rafts. *Nat. Rev. Mol. Cell Biol.* **18**, 361-374. doi:10.1038/nrm.2017.16

Shutova, M. S., Spessott, W. A., Giraudo, C. G. and Svitkina, T. (2014). Endogenous species of mammalian nonmuscle myosin IIA and IIB include activated monomers and heteropolymers. *Curr. Biol.* **24**, 1958-1968. doi:10.1016/j.cub.2014.07.070

Small, J. V., Stradal, T., Vignal, E. and Rottner, K. (2002). The lamellipodium: where motility begins. *Trends Cell Biol.* **12**, 112-120. doi:10.1016/S0962-8924(01)02237-1

Straight, A. F., Cheung, A., Limouze, J., Chen, I., Westwood, N. J., Sellers, J. R. and Mitchison, T. J. (2003). Dissecting temporal and spatial control of cytokinesis with a myosin II Inhibitor. *Science* **299**, 1743-1747. doi:10.1126/science.1081412

Tinevez, J. Y., Schulze, U., Salbreux, G., Roensch, J., Joanny, J. F. and Paluch, E. (2009). Role of cortical tension in bleb growth. *Proc. Natl. Acad. Sci. USA* **106**, 18581-18586. doi:10.1073/pnas.0903353106

Titus, M. A. (2017). Growing, splitting and stacking myosin II filaments. *Nat. Cell Biol.* **19**, 77-79. doi:10.1038/ncb3468

Totsukawa, G., Yamakita, Y., Yamashiro, S., Hartshorne, D. J., Sasaki, Y. and Matsumura, F. (2000). Distinct roles of ROCK (Rho-kinase) and MLCK in spatial regulation of MLC phosphorylation for assembly of stress fibers and focal adhesions in 3T3 fibroblasts. *J. Cell Biol.* **150**, 797-806. doi:10.1083/jcb.150.4.797

Vicente-Manzanares, M., Choi, C. K. and Horwitz, A. R. (2009a). Integrins in cell migration–the actin connection. *J. Cell Sci.* **122**, 199-206. doi:10.1242/jcs.018564

Vicente-Manzanares, M., Ma, X., Adelstein, R. S. and Horwitz, A. R. (2009b). Non-muscle myosin II takes centre stage in cell adhesion and migration. *Nat. Rev. Mol. Cell Biol.* **10**, 778-790. doi:10.1038/nrm2786

Wu, D., Asiedu, M. and Wei, Q. (2009). Myosin-interacting guanine exchange factor (MyoGEF) regulates the invasion activity of MDA-MB-231 breast cancer cells through activation of RhoA and RhoC. *Oncogene* **28**, 2219-2230. doi:10.1038/onc.2009.96

Zhang, X.-F., Ajeti, V., Tsai, N., Fereydooni, A., Burns, W., Murrell, M., de la Cruz, E. M. and Forscher, P. (2019). Regulation of axon growth by myosin II-dependent mechanocatalysis of cofilin activity. *J. Cell Biol.* **218**, 2329-2349. doi:10.1083/jcb.201810054

Time lapse images were captured at 20 sec intervals for 30-75 min and all movies play at 10 fps.

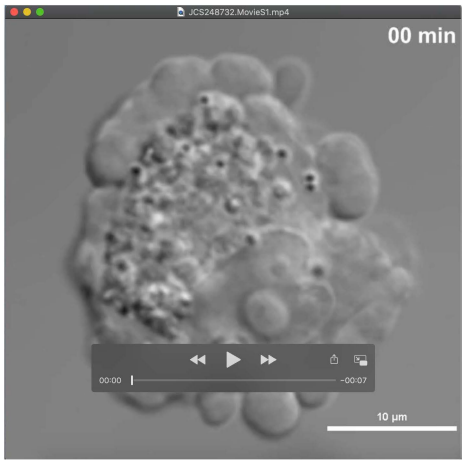

Movie 1. Blebbing MDA-MB-231 cell treated with 30 µM (-) blebbistatin.

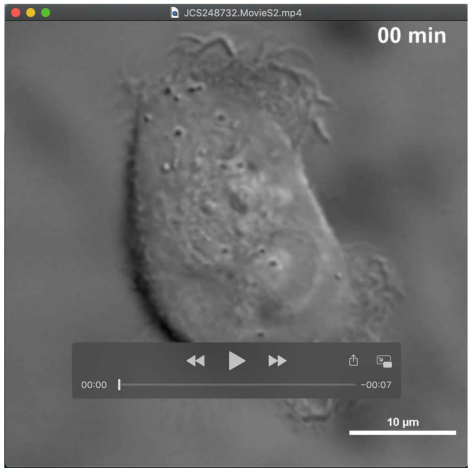

Movie 2. Lamellipodia MDA-MB-231 cell treated with 30 µM (-) blebbistatin.

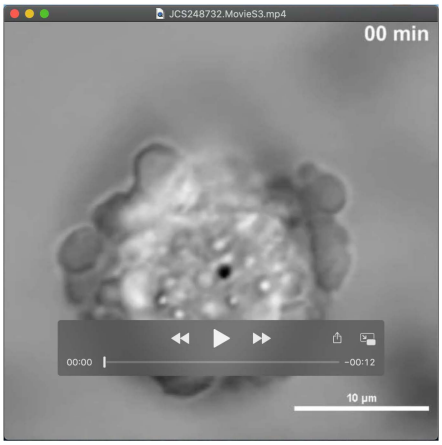

Movie 3. Blebbing MDA-MB-231 cell treated with 30 µM (-) blebbistatin & its washout.

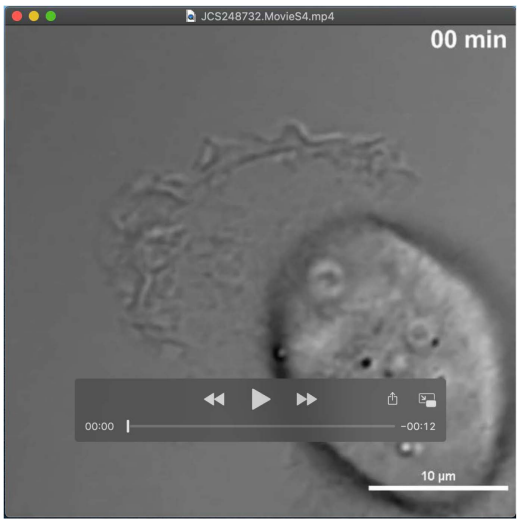

Movie 4. Lamellipodia MDA-MB-231 cell treated with 30 µM (-) blebbistatin & its washout.

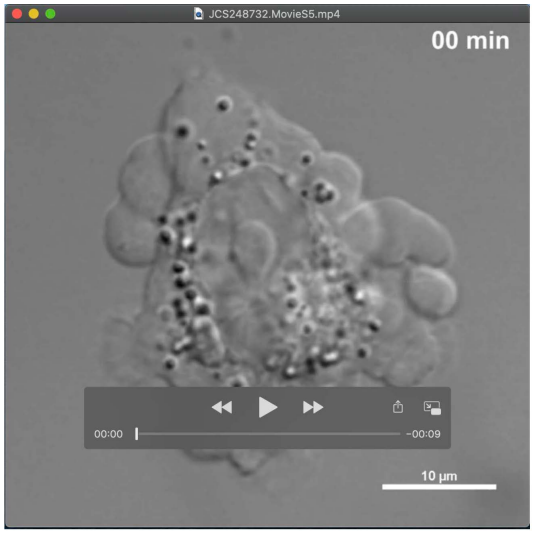

Movie 5. Blebbing MDA-MB-231 cell treated with 2.5 µM (-) blebbistatin.

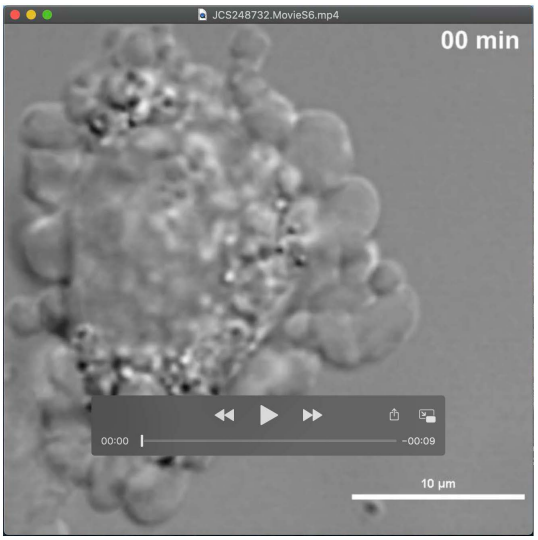

Movie 6. Blebbing MDA-MB-231 cell treated with 1 µM (-) blebbistatin.

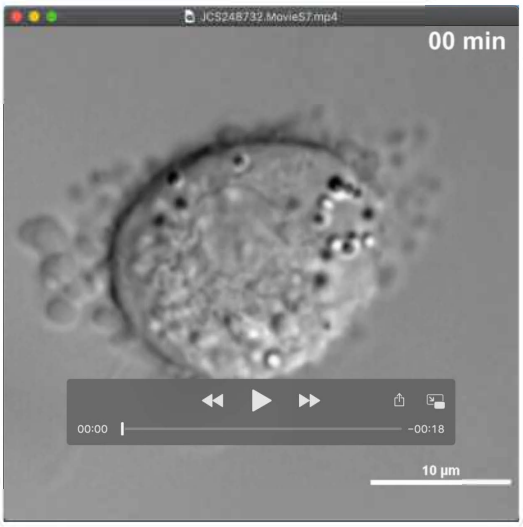

Movie 7. Blebbing MDA-MB-231 cell treated with 2.5 µM (-) blebbistatin & its washout.

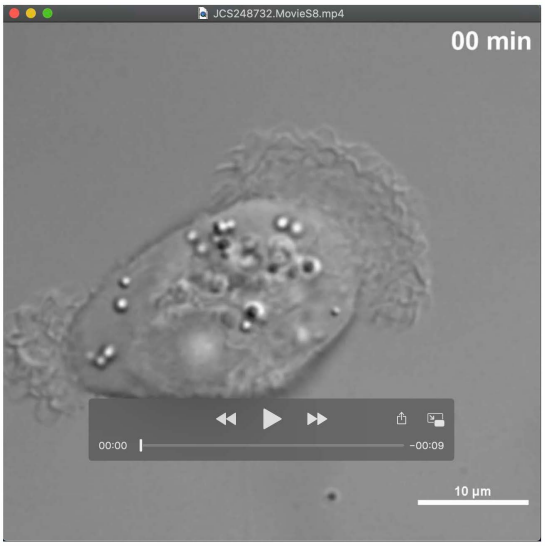

Movie 8. Lamellipodia MDA-MB-231 cell treated with 2.5 µM (-) blebbistatin.

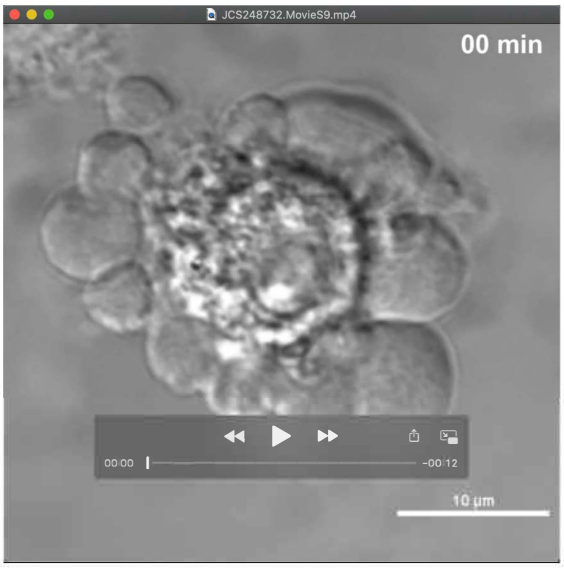

Movie 9. Blebbing MDA-MB-231 cell treated with 10 µM (-) blebbistatin.

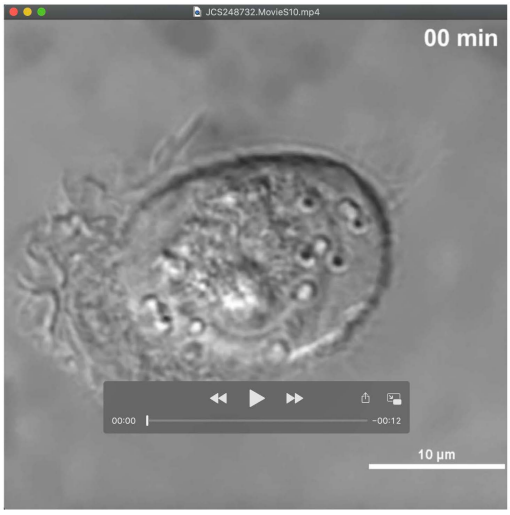

Movie 10. Lamellipodia MDA-MB-231 cell treated with 10 µM (-) blebbistatin.

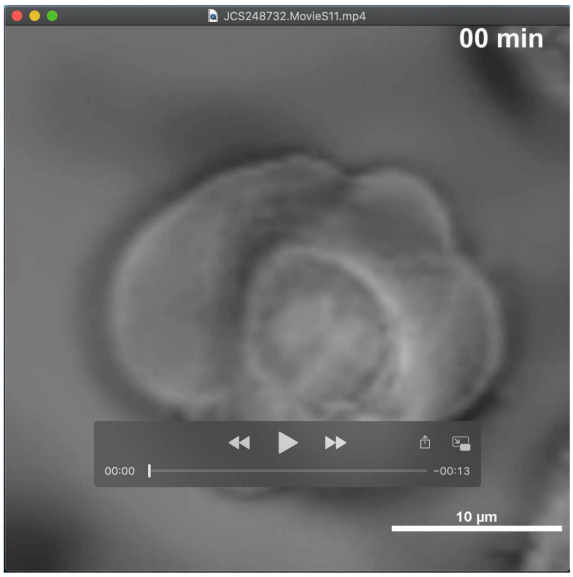

Movie 11. Blebbing MDA-MB-231 cell treated with 10 µM (-) blebbistatin & its washout.

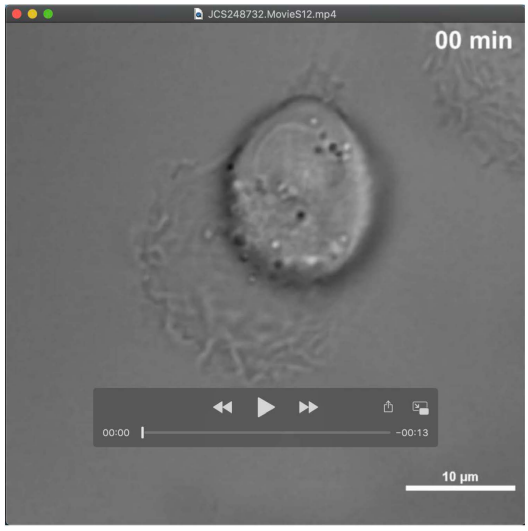

Movie 12. Lamellipodia MDA-MB-231 cell treated with 10 µM (-) blebbistatin & its washout.

Journal of Cell Science • Supplementary information

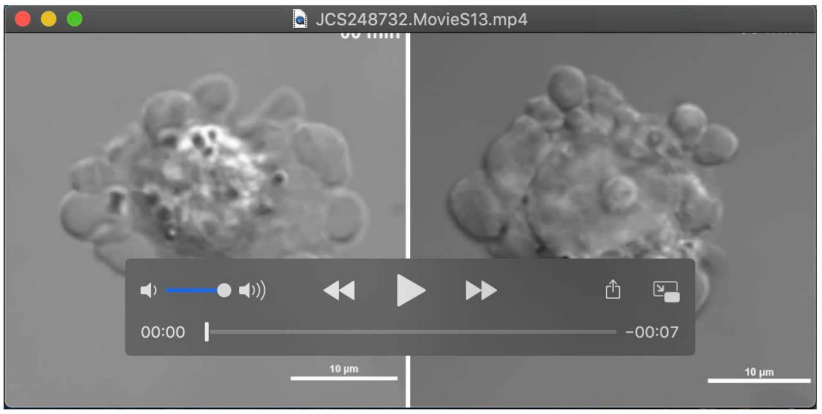

Movie 13. Blebbing MDA-MB-231 cell treated with 0.2% DMSO or 2.5 µM (+) blebbistatin.

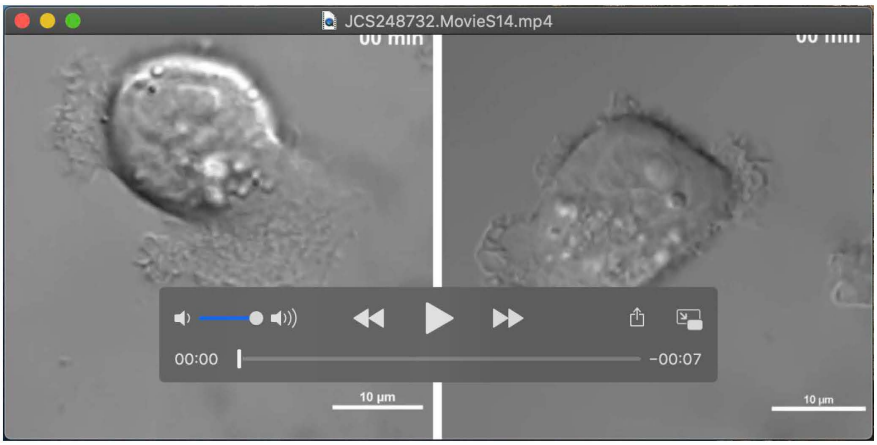

Movie 14. Lamellipodia MDA-MB-231 cell treated with 0.2% DMSO or 2.5 µM (+) blebbistatin.

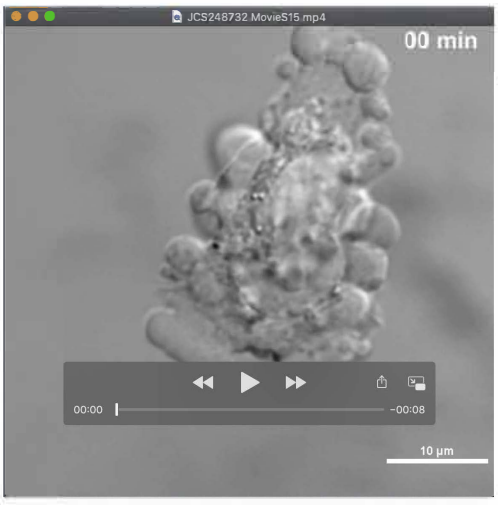

Movie 15. Blebbing MDA-MB-231 cell treated with 5µM Y27632.

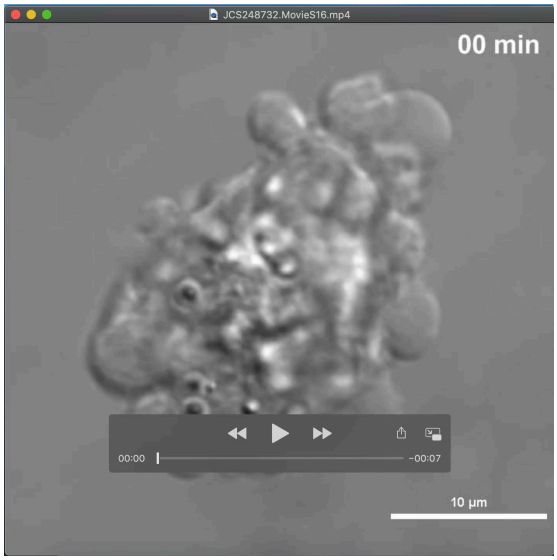

Movie 16. Blebbing MDA-MB-231 cell treated with 20µM Y27632.

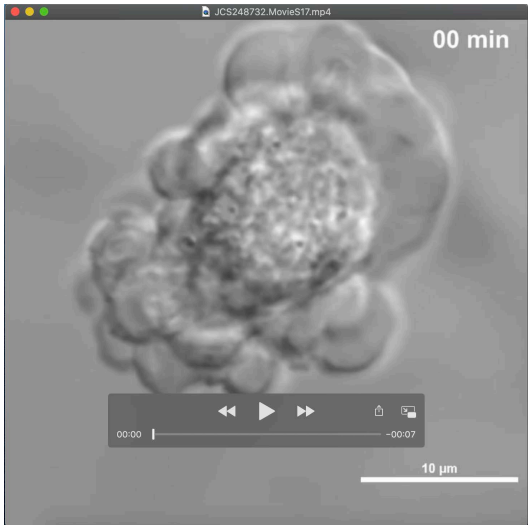

Movie 17. Blebbing MDA-MB-231 cell treated with 5 µM ML7.

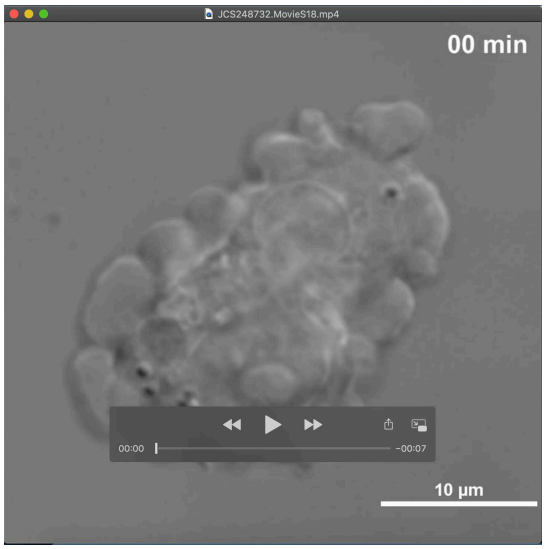

Movie 18. Blebbing MDA-MB-231 cell treated with 20 µM ML7.

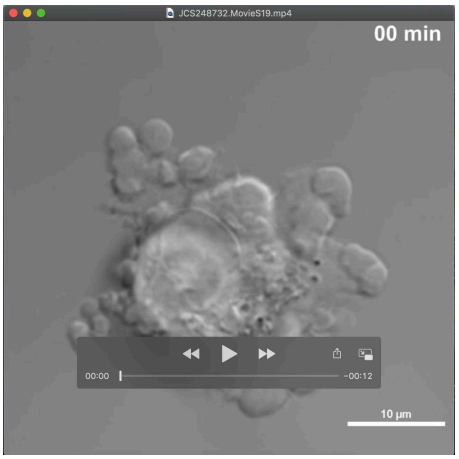

Movie 19. Blebbing MDA-MB-231 cell treated with 5 µM Y27632 & its washout.

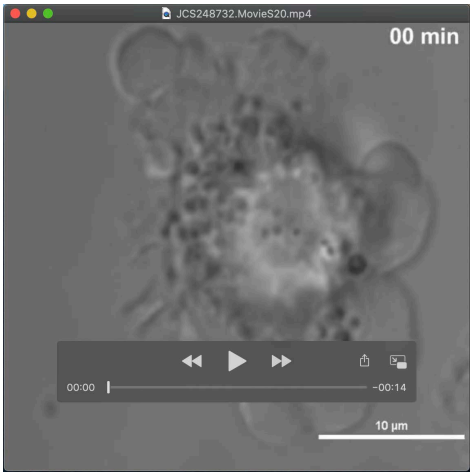

Movie 20. Blebbing MDA-MB-231 cell treated with 20 µM Y27632 & its washout.

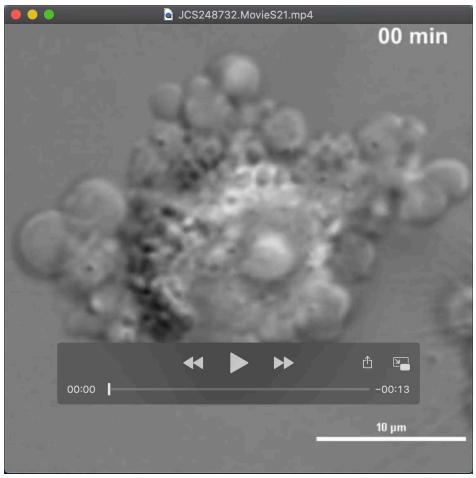

Movie 21. Blebbing MDA-MB-231 cell treated with 20 µM ML7 & its washout.

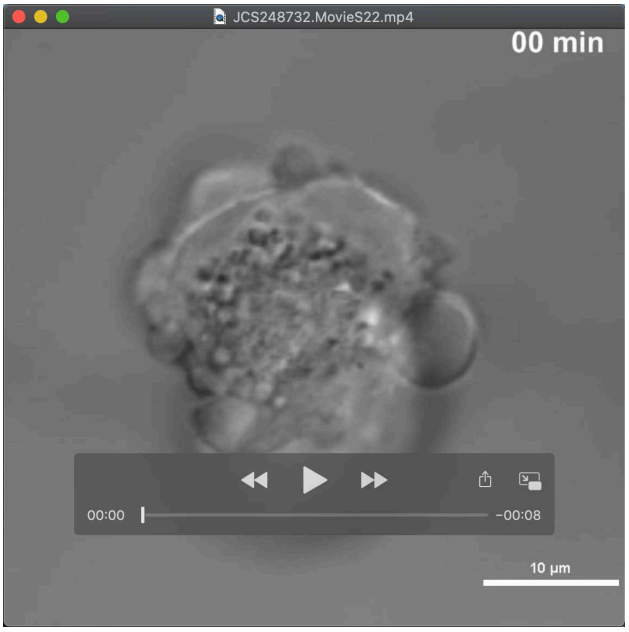

Movie 22. Blebbing MDA-MB-231 cell treated with 0.1 µM Y27632.

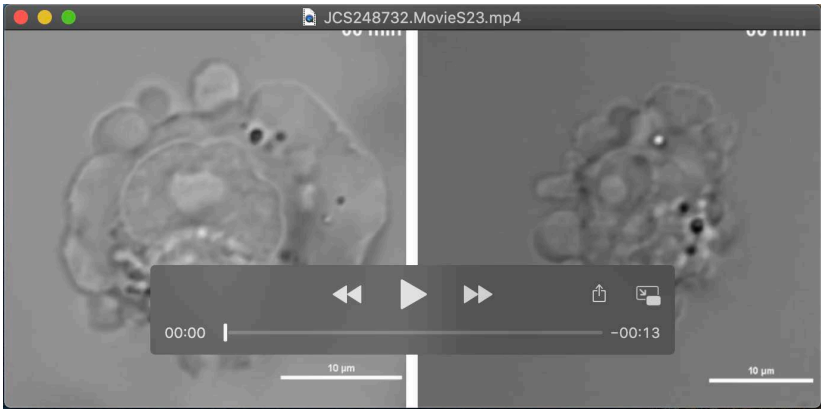

Movie 23. Blebbing MDA-MB-231 cell treated with1or 2 µM Y27632& their washout.

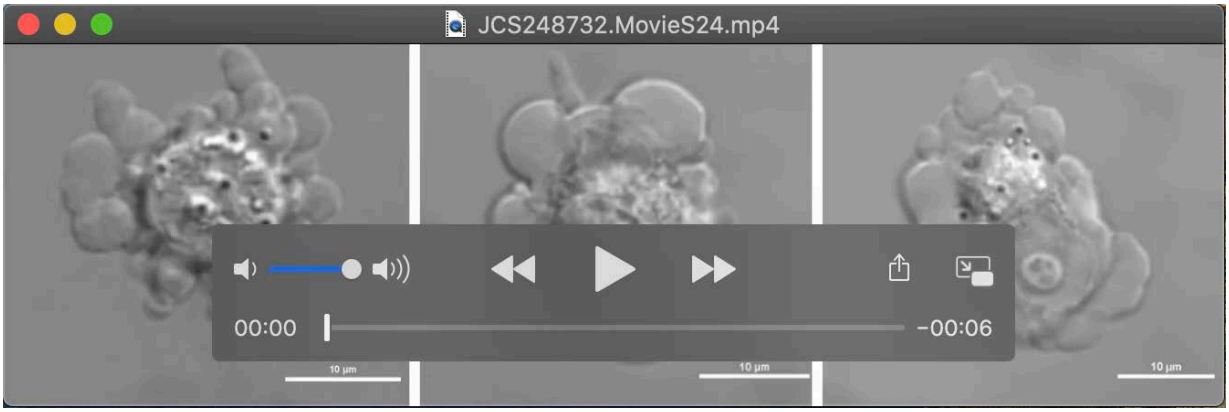

Movie 24. Blebbing MDA-MB-231 cell treated with 20 µM TBBt, 20 µM Go6976, or 20 µM TG100-115.

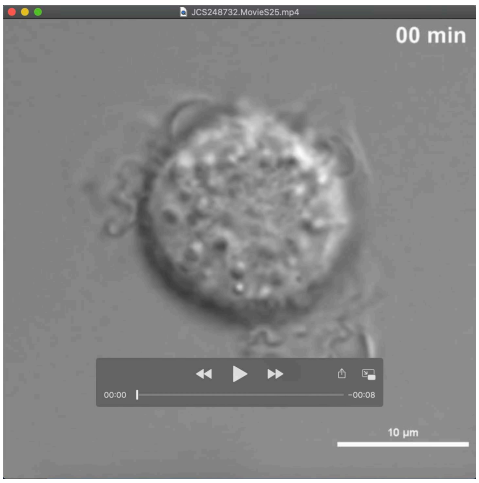

Movie 25. Lamellipodia MDA-MB-231 cell treated with 30 µM Y27632.

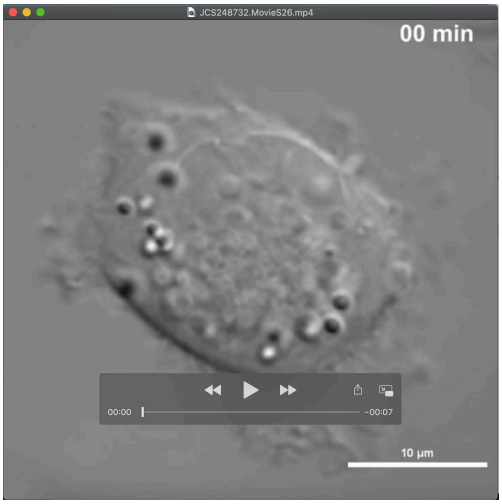

Movie 26. Lamellipodia MDA-MB-231 cell treated with 5 µM ML7.

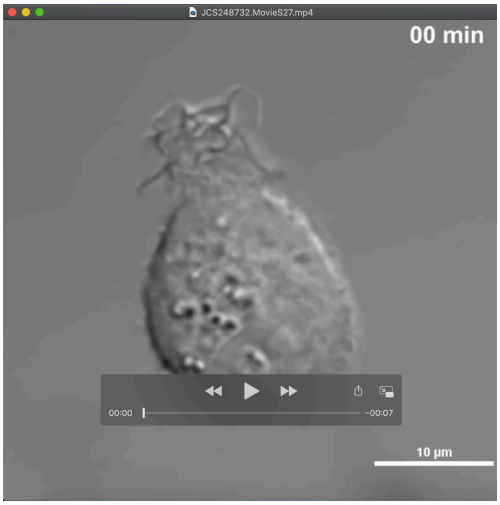

Movie 27. Lamellipodia MDA-MB-231 cell treated with 10 µM ML7.

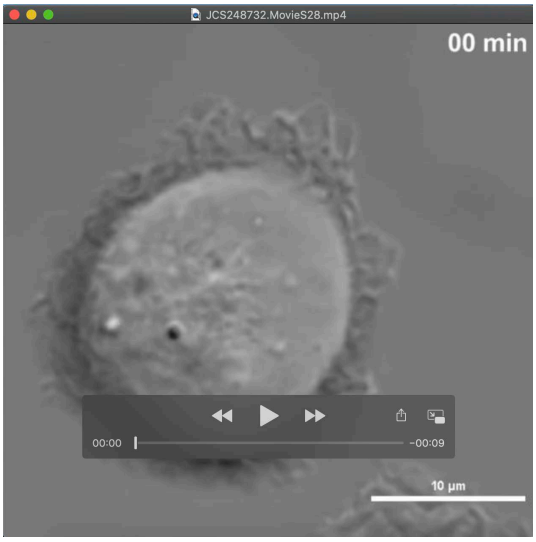

Movie 28. Lamellipodia MDA-MB-231 cell treated with 10 µM ML7 and its washout.

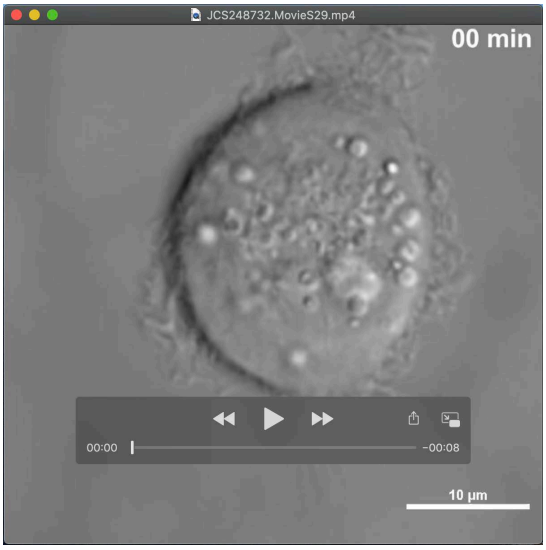

Movie 29. Lamellipodia MDA-MB-231 cell treated with 20 µM ML7.

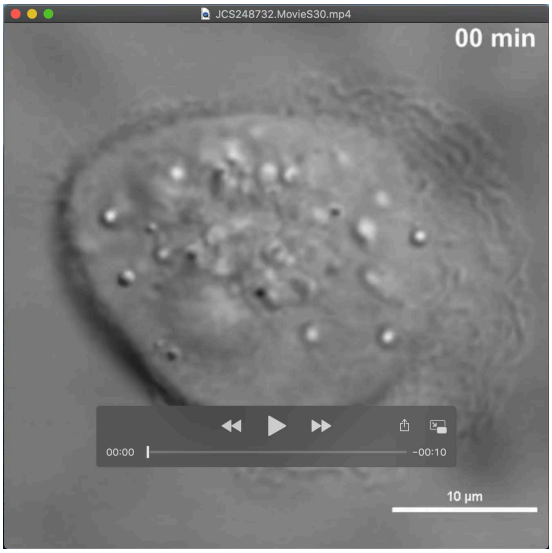

Movie 30. Lamellipodia MDA-MB-231 cell treated with 20 µM ML7 and its washout.

Movie 31. Lamellipodia MDA-MB-231 cell treated with 20 µM TBBt, 20 µM Go6976, or 20 µM TG100-115.

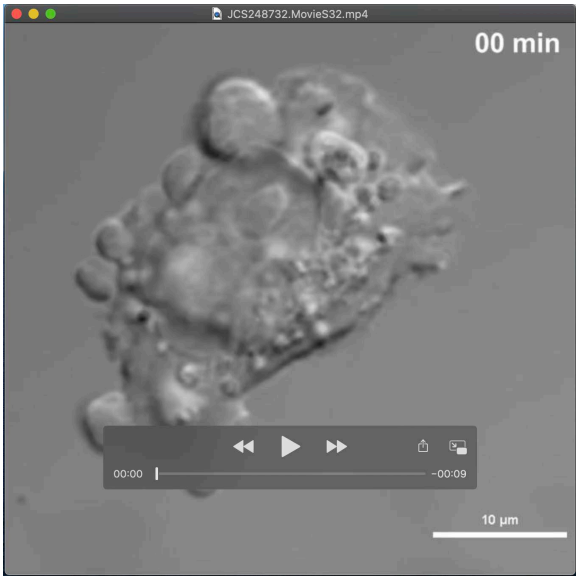

Movie 32. Blebbing MDA-MB-231 cell treated with 5 µM Y27632 and then with 10 µM ML7.

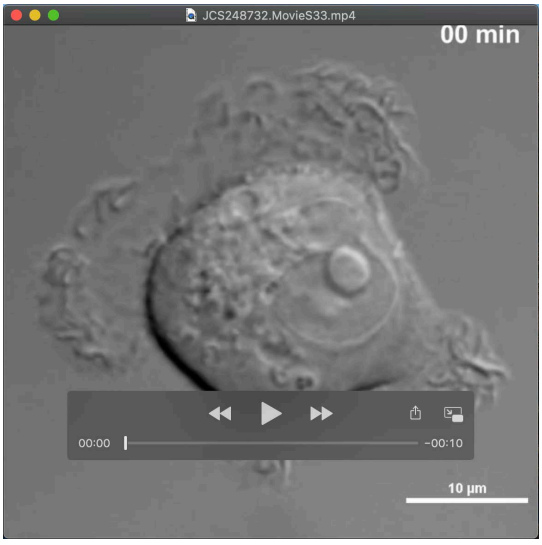

Movie 33. Lamellipodia MDA-MB-231 cell treated with 5 µM Y27632 and then with 10 µM ML7.

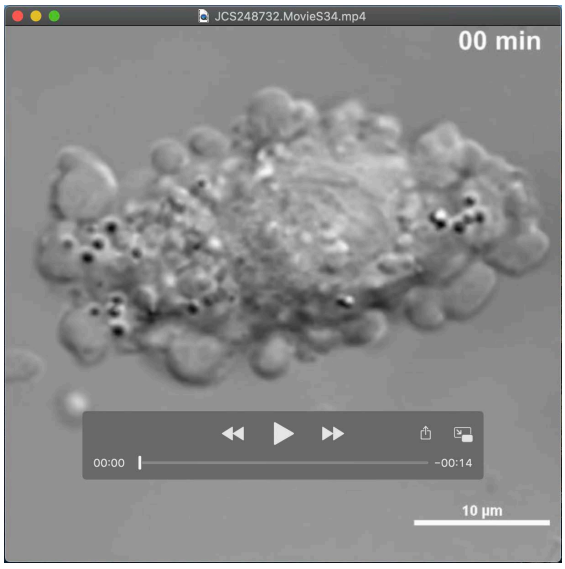

Movie 34. Blebbing MDA-MB-231 cell treated with 10 µM ML7 and then with 5 µM Y27632.

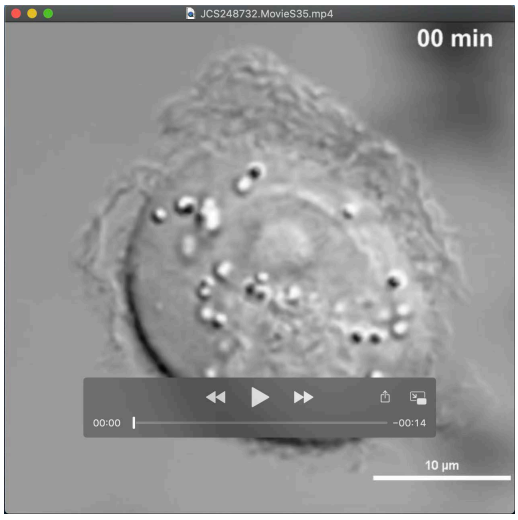

Movie 35. Lamellipodia MDA-MB-231 cell treated with 10 µM ML7 and then with 5 µM Y27632.

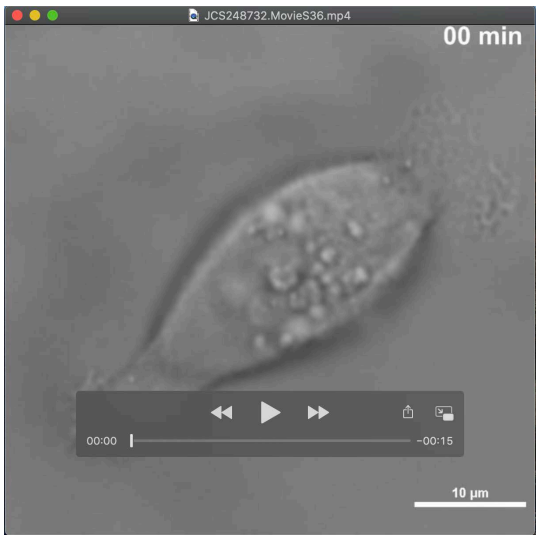

Movie 36. Lamellipodia MDA-MB-231 cell treated with 30 µM CK666 and its washout.

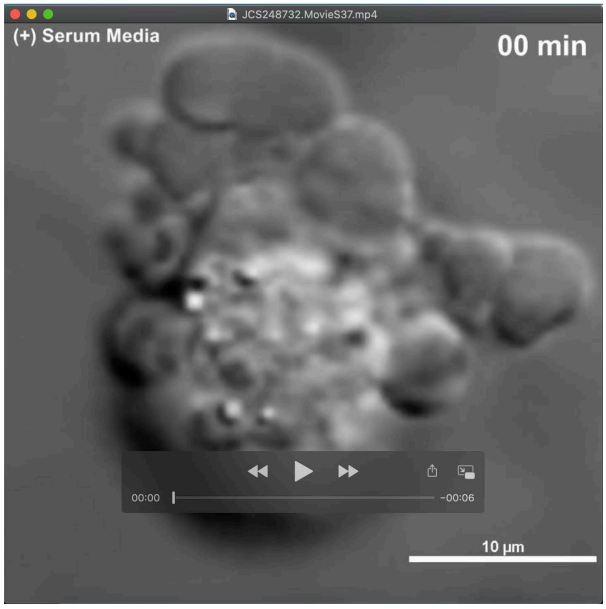

Movie 37. Blebbing MDA-MB-231 cell under serum starvation.

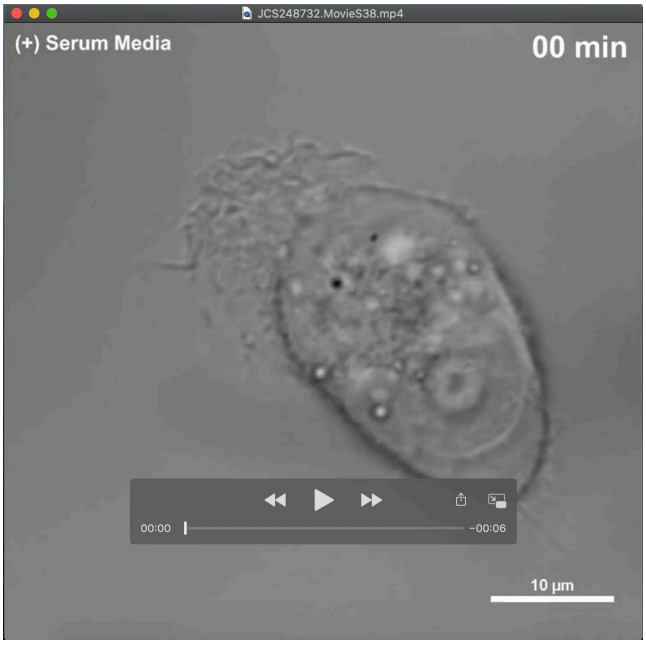

Movie 38. Lamellipodia MDA-MB-231 cell under serum starvation.

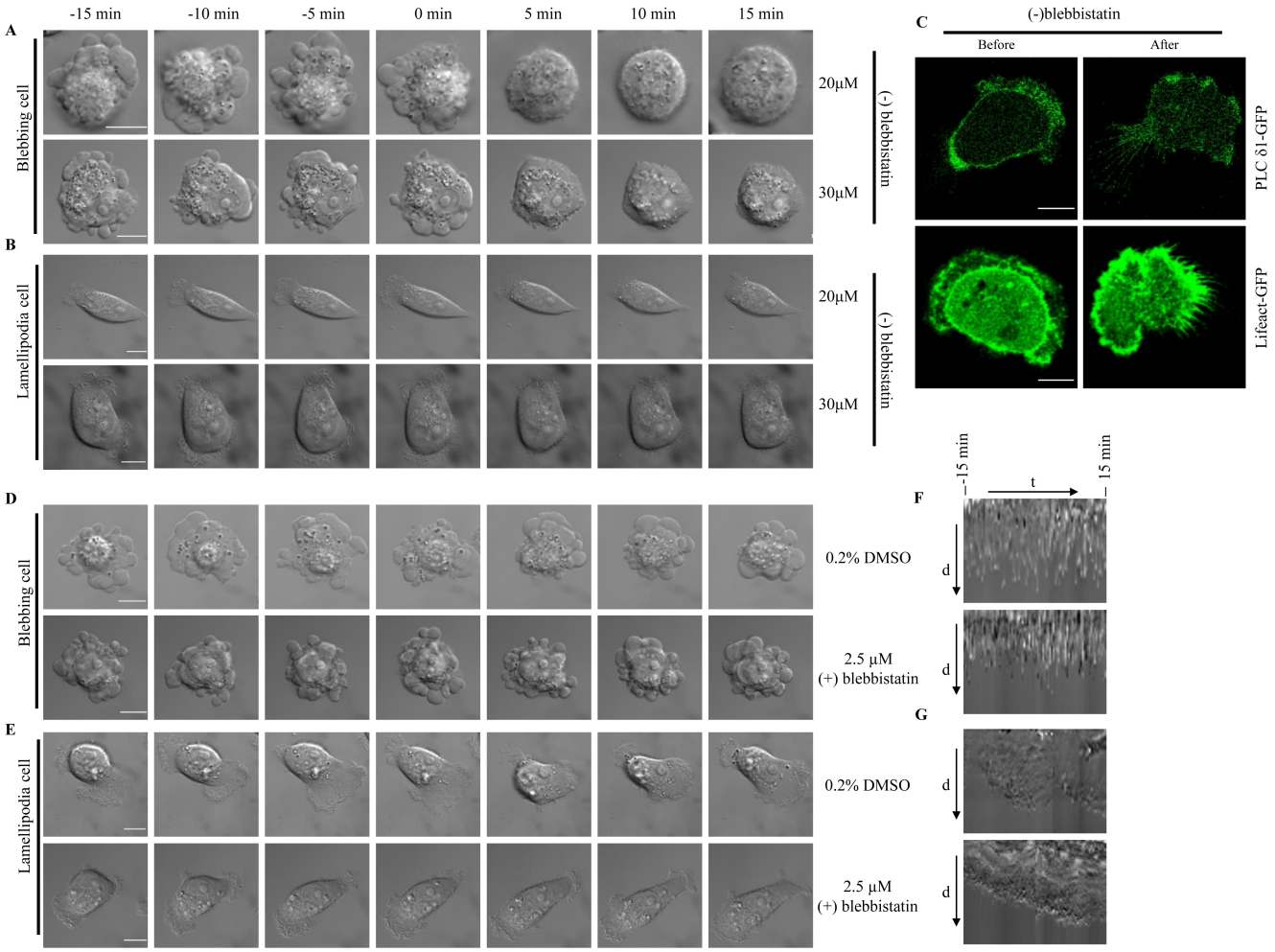

Figure S1

Figure S1 Blebbing and lamellipodia membrane protrusions are NMII dependent.(A-B), Time lapse images of blebbing (A) and lamellipodia (B) MDA-MB-231 cells treated with 20 & 30 µM (-) blebbistatin. Images were captured for 15 min before and for 15 min after the addition of inhibitor. Note that both blebbing and lamellipodia cells stop their membrane protrusion activity within 5-10 min of addition. n≥ 20 cells for each treatment from three independent experiments (C), Representative confocal fluorescent images of 10 µM (-) blebbistatin treated lamellipodia MDA-MB-231 cells which were transfected with PLC δ1-GFPor Lifeact-GFP. Time lapse images of blebbing (D) and lamellipodia (E) MDA-MB-231 cells treated with 0.2% DMSO or 2.5 µM (+) blebbistatin. (F-G) The representative DIC kymographs of 0.2% DMSO or (+) blebbistatin treated blebbing (F) and lamellipodia (G). Note that both blebbing and lamellipodia membrane protrusions were not affected in presence of inactive enantiomer of (-) blebbistatin or vehicle control 0.2% DMSO.Scale bar: 10µm

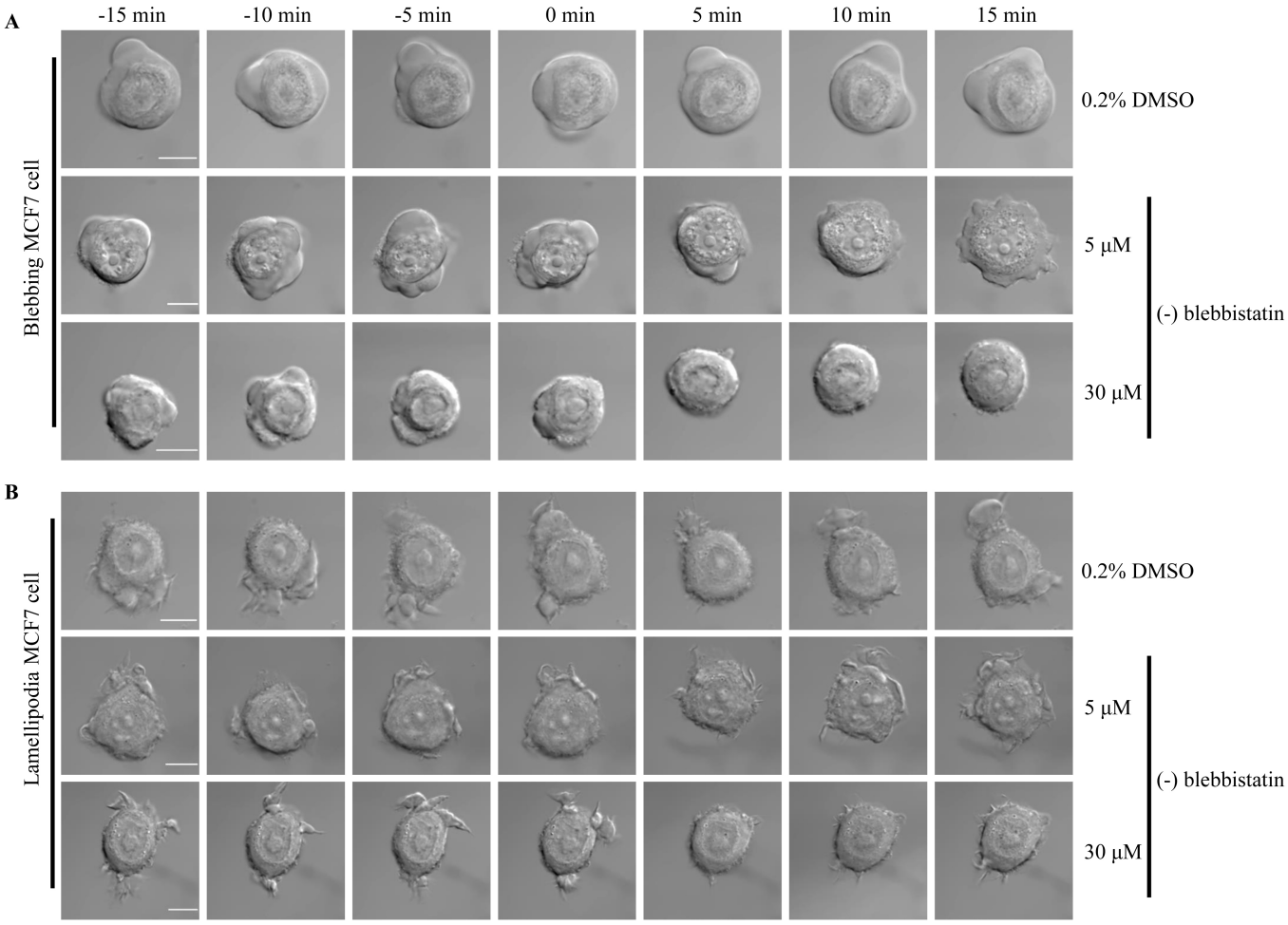

Figure S2

Figure S2 Blebbing to lamellipodia conversion (BLC) of (-) blebbistatin treated MCF-7 cells. (A-B), Snap shots of time lapse movies of blebbing (A) and lamellipodia (B) MCF-7 cells treated with 0.2% DMSO, 5µM or 30 µM (-) blebbistatin. Note that treatment of 5 µM (-) blebbistatin converts blebbing to lamellipodia whereas that of 30 µM (-) blebbistatin stops blebbing within 5 min. n≥ 10 cells for each doses from three independent experiments. Scale bar: 10µm

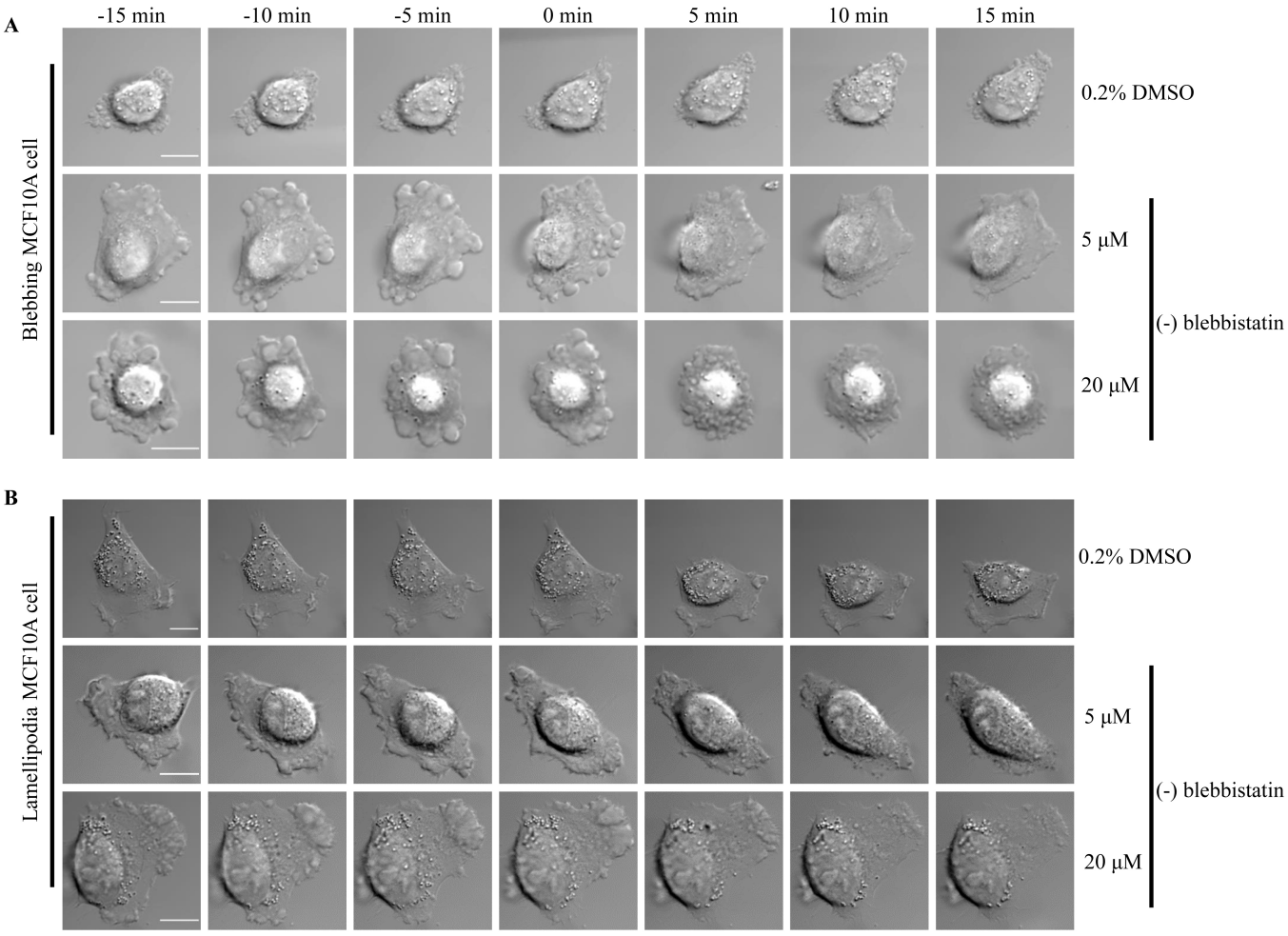

Figure S3

Figure S3 Blebbing to lamellipodia conversion (BLC) of (-) blebbistatin treated MCF10A cells. (A-B) Time lapse images of blebbing (A) and lamellipodia (B) MCF10A cells treated with 0.2% DMSO, 5µM or 20 µM (-) blebbistatin. Note that blebbing to lamellipodia conversion was visible in the presence of 5 µM (-) blebbistatin whereas20 µM (-) blebbistatin stops blebbing within 5 min. Similar to Sup fig 3, lamellipodia remain unchanged in the presence of 5 µM (-) blebbistatin but stopped with 20 µM (-) blebbistatin. n≥ 10 cells for each doses from three independent experiments. Scale bar: 10µm

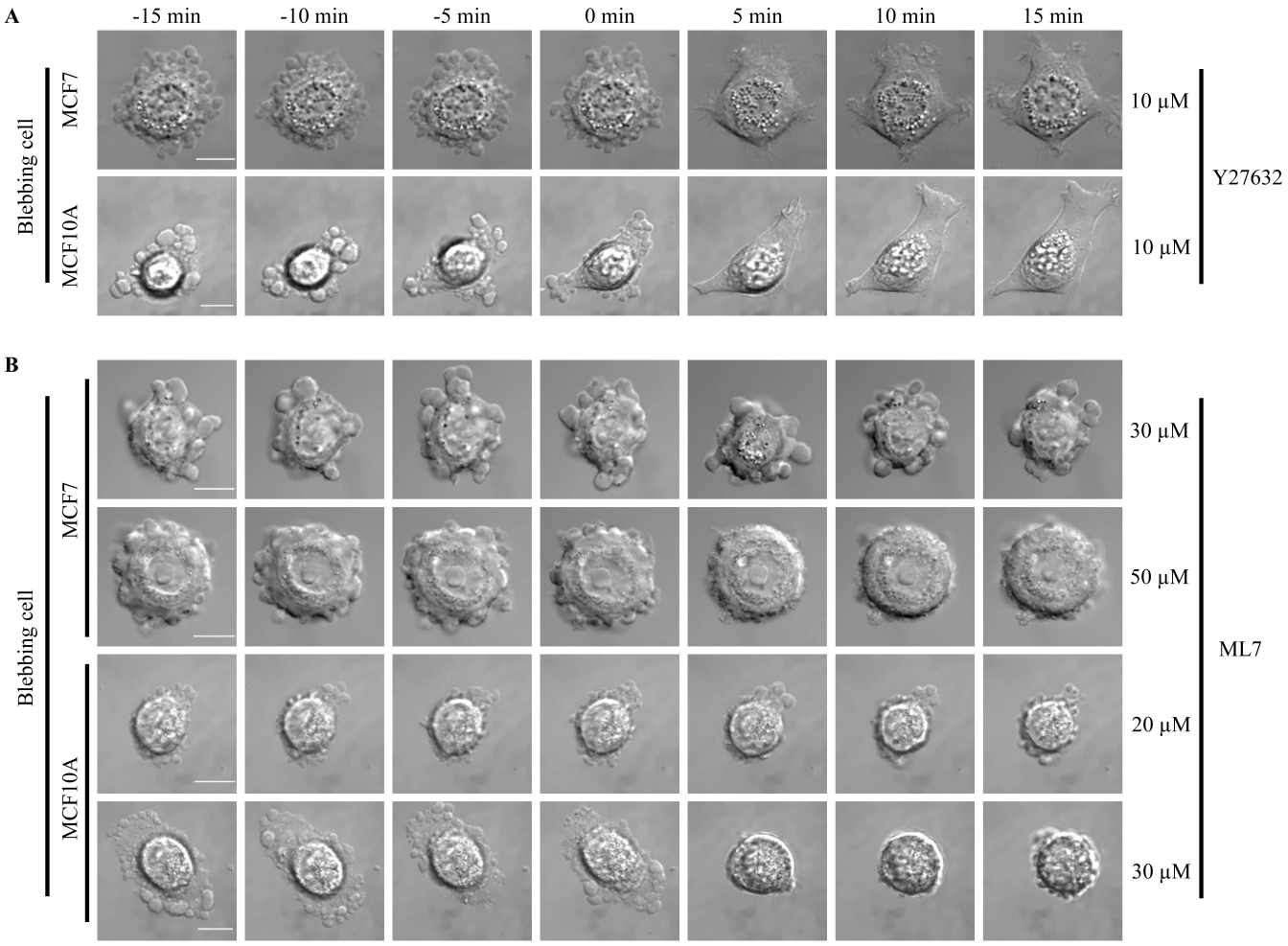

Figure S4

Figure S4 Blebbing to lamellipodia conversion (BLC) of Y27632 treated MCF7 and MCF10A cells. (A-B), Time lapse images of blebbing MCF7 and MCF10A cells treated with 10 μM Y27632 (A) or 20-50 μM ML7 (B). Note that blebbing of both MCF7 and MCF10A cells were converted into lamellipodia in the presence of 10 μM Y27632, whereas stopped in the presence of ≥ 30 μM ML7. n≥ 10 cells for each doses from three independent experiments. Scale bar: 10μm

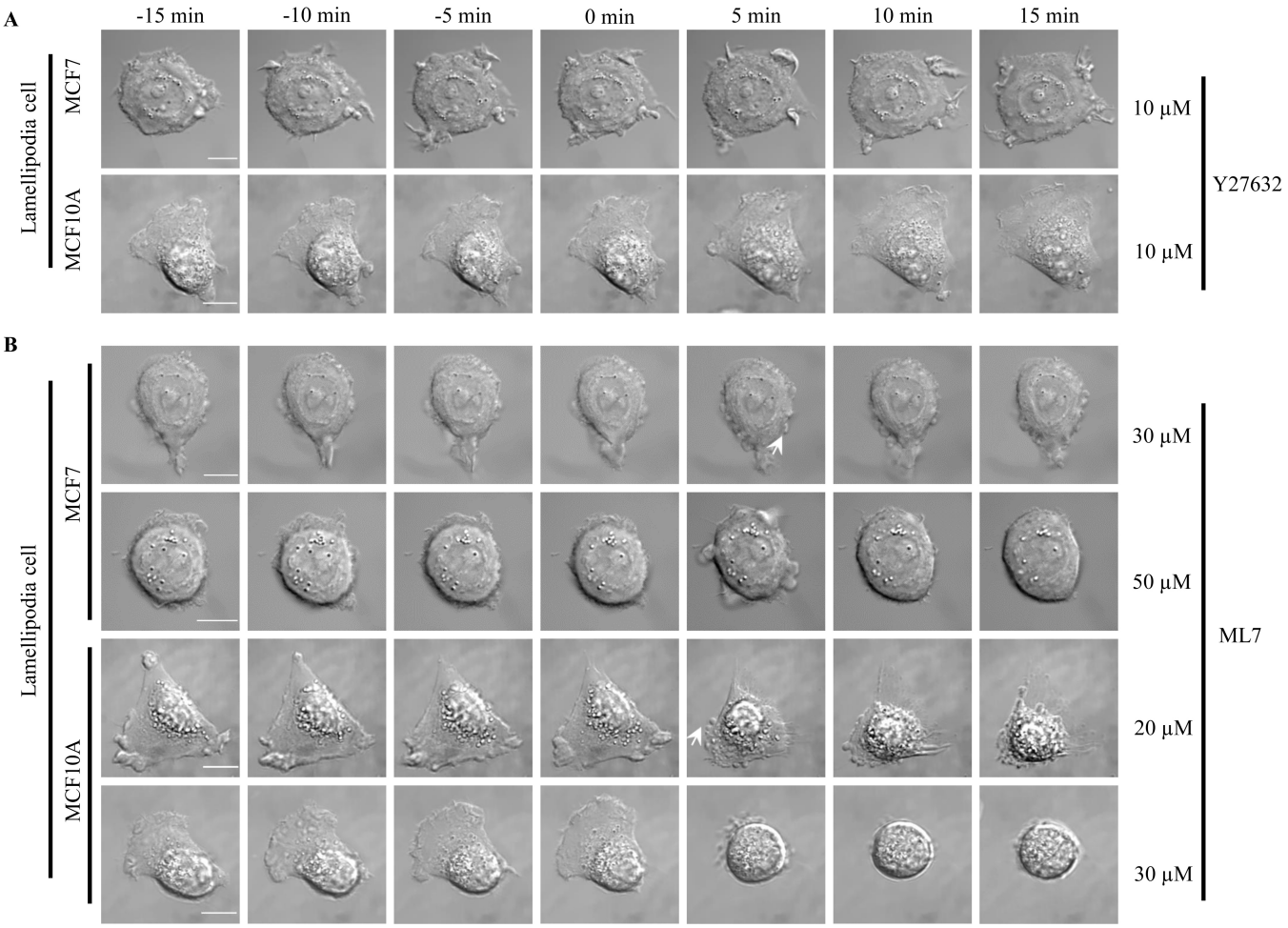

Figure S5

Figure S5 Lamellipodia to blebbing conversion (LBC) of ML7 treated MCF7 and MCF10A cells**.** (A-B), Time lapse images of Lamellipodia MCF7 and MCF10A cells treated with 10 µM Y27632 (A) or 20-50 µM ML7 (B). Note that lamellipodia of both MCF7 and MCF10A cells were not affected in presence of Y27632, but converted to blebbing in the presence of ML7. Arrows indicate the appearance of blebs. n≥ 10 cells for each dose for each cell types from three independent experiments. Scale bar: 10µm

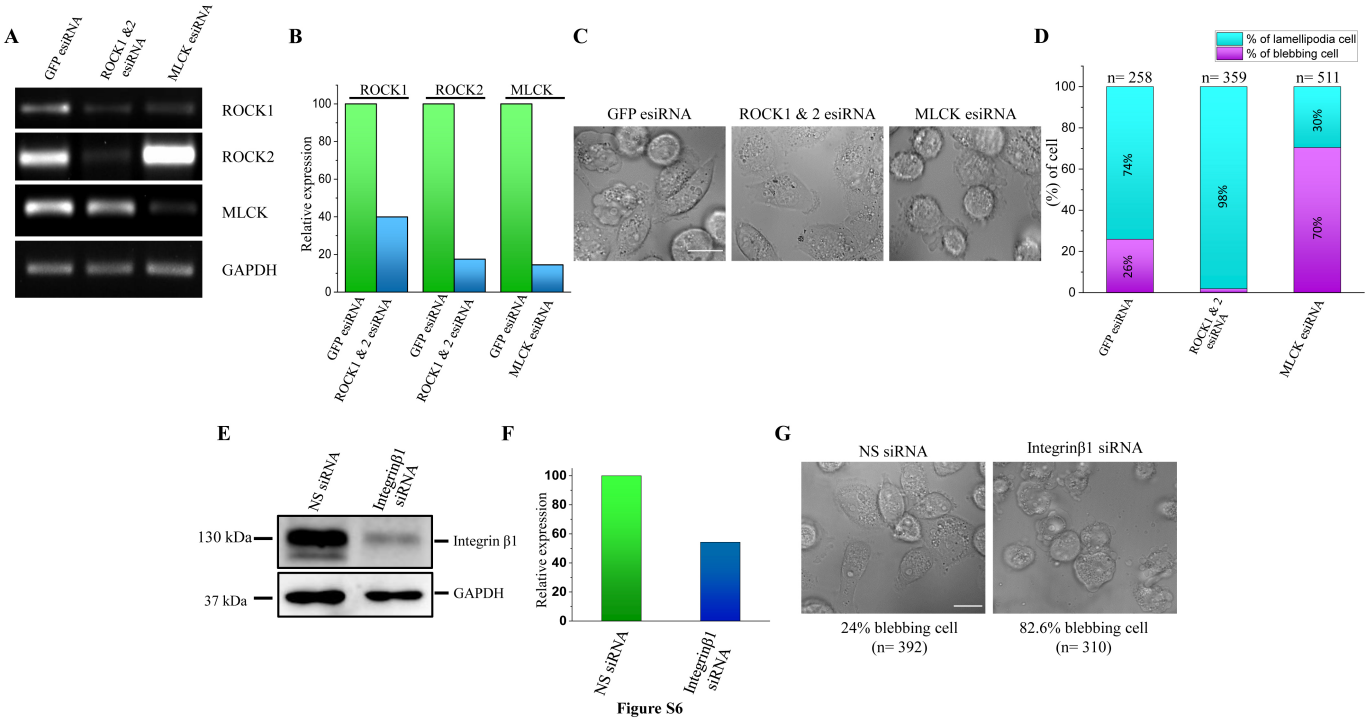

Figure S6

Figure S6 Effect of ROCK, MLCK, and Integrinβ1 knockdown in MDA-MB-231 cells. (A) Total RNA isolated from GFP, ROCK1&2 or MLCK esiRNA treated cells was reverse transcribed and checked for the expression of ROCK1&2 and MLCK using specific primers. GAPDH was considered as loading control. A representative image from two independent experiments. (B) Average of fold intensity from n=2 experiments. Fold intensity was calculated considering relative band intensity (intensity of band of interest/intensity of GAPDH band) of GFPesiRNA treated sample as "100". (C) Representative DIC images of NS, ROCK or MLCK esiRNA treated cells. (D) Quantification of cells showing blebbing or lamellipodia in GFP, ROCK1&2 or MLCK esiRNA treated cells (n≥250, from two independent experiments). (E) Immunoblot analysis with integrin β1 and GAPDH antibodies of NS or integrin β1 siRNA treated MDA-MB-231 cells. (F) Average of fold intensity from n=2 experiments. (G) Representative DIC image of NS or integrinβ1siRNA treated cells. Quantification of % of blebbing cells (n≥ 300, from two independent experiments) shown below the images. Scale bar: 20µm

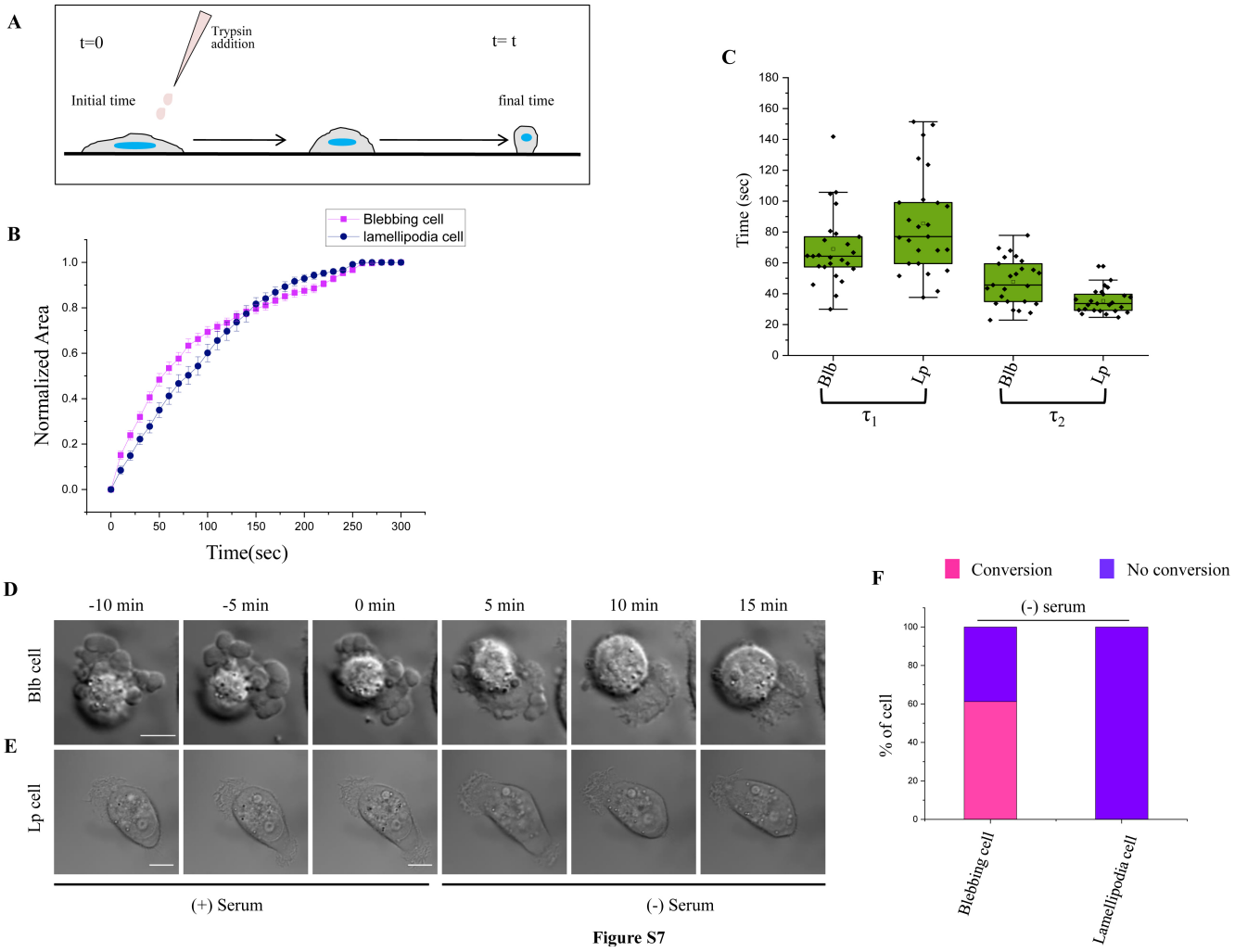

Figure S7

Figure S7 Contractility difference between blebbing and lamellipodia cells. (A) Schematic diagram of trypsin de-adhesion assay. At t=0, cells were washed with PBS and incubated with trypsin and images were captured at 10 sec intervals until cell became rounded. (B) Quantification of cell area changes during de-adhesion. (C) Quantification of the time constants (τ_1, τ_2) of blebbing and lamellipodia cells. n≥ 25 cells for each type of cell from three independent experiments. Time lapse images of blebbing (D) and lamellipodia (E) MDA-MB-231 cells under serum starvation. Images were captured for 10 min before and for 15 min after the serum starvation. Note that only blebbing cell converts to lamellipodia under serum starvation whereas lamellipodia cell does not show any conversion. n≥ 40 cells for each type of cells from three independent experiments. (F), Quantification of conversion of blebbing and lamellipodia cell under serum starvation.Scale bar: 10µm

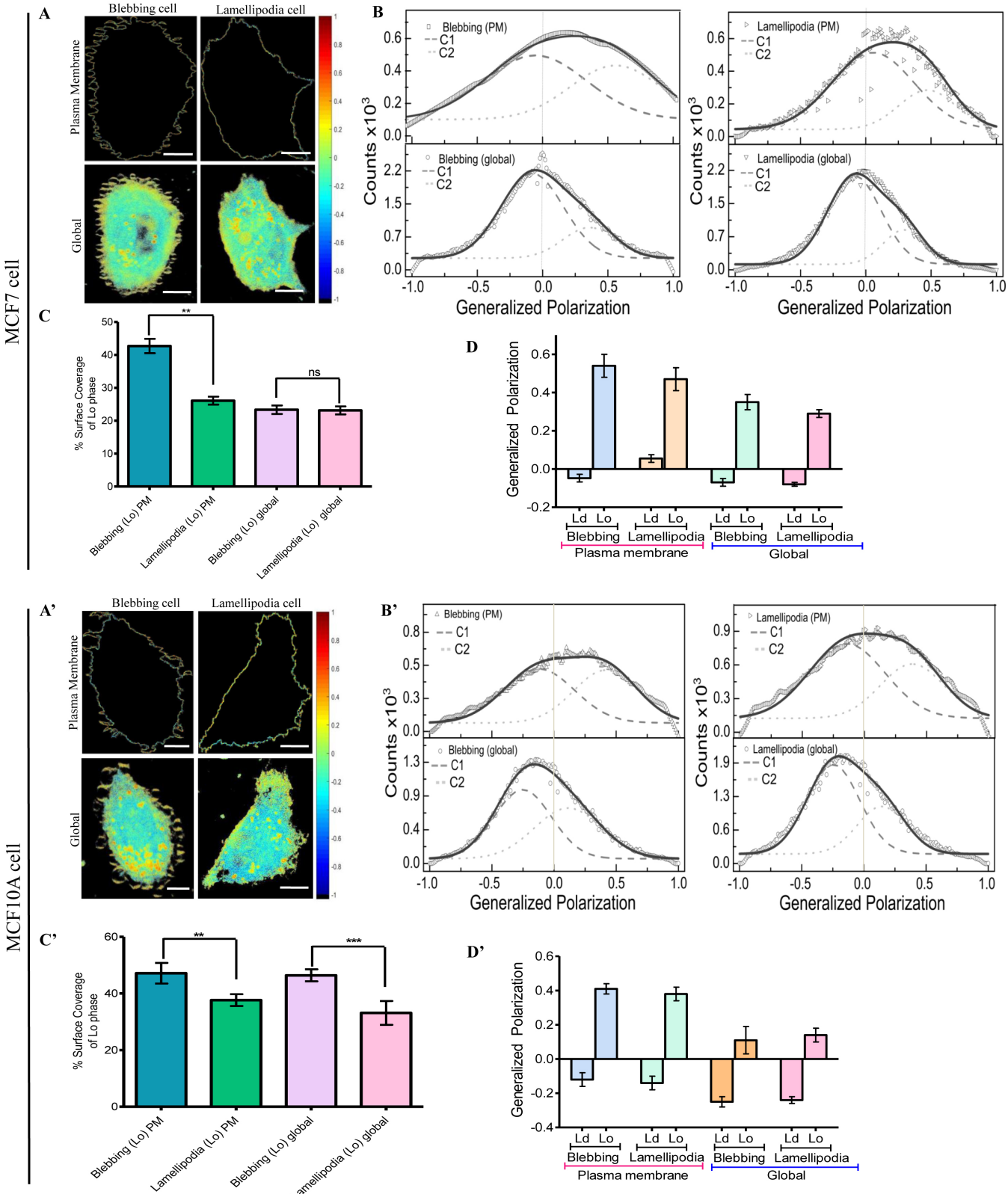

Figure S8

Figure S8 MCF7 and MCF10A cell distinctly changes the fluidity and lipid order (Lo) of blebbing and lamellipodia membrane. (A, A') Pseudo-colored GP images of global and plasma membrane of blebbing and lamellipodia. (B, B'), Associated global and plasma membrane of segmented GP distribution from the stack of GP images (n = 30, N= 3) deconvoluted by fitting two-Gaussian distributions. (C, C') Percentage of surface coverage of Lo phase distributed in normalized GP distribution that expressed as area under the curve of two Gaussian distribution, represented in bar graph. Data are mean ± SEM from three independent experiments and were statistically analysed using the two-tailed student's t-test (**$P< 0.05$). (D, D') Lipid order and fluidity (Generalized Polarization) of cellular membrane, represented in bar graph. Scale bar: 10µm